Development of a field water/cement ratio test using time domain reflectometry

by

Binxiang Yu

B.S., Kansas State University, 2024

A THESIS

submitted in partial fulfillment of the requirements for the degree

MASTER OF SCIENCE

Department of Civil Engineering
Carl R. Ice College of Engineering

KANSAS STATE UNIVERSITY
Manhattan, Kansas

2025

Approved by:

Co-Major Professor
Juan Du

Approved by:

Co-Major Professor
Mustaque Hossain

Abstract

A reliable and nondestructive method is needed to determine the water-to-cement or water-to-cementitious material ratio (w/cm) of fresh concrete for performance-based quality assurance. This study developed and validated a Time Domain Reflectometry (TDR) based method to quantify the real-time w/cm ratio of fresh concrete. Forty-eight concrete mixtures with varying w/cm ratios, air contents, and cementitious binder types (cement-only, fly ash, and slag) were tested, and TDR measurements were synchronized with conventional tests to establish a calibrated model between the apparent dielectric constant (K_a) and volumetric water content (θ_v). Data were analyzed using the statistical software R, employing group standardization, ordinary least-squares regression, and the Simulation–Extrapolation (SIMEX) method to correct for measurement-error bias. Four models developed for different cementitious binder systems showed strong consistency between measured and predicted results, confirming the reliability of the proposed calibration framework. However, as an empirical model, its applicability may be limited to the specific material range for which it was tested. Future studies should incorporate additional laboratory and field experiments, as well as explore physics-based dielectric modeling, to enhance prediction accuracy and generalization.

Table of Contents

Table of Contents iii
List of Figures vi
List of Tables vii
Chapter 1: Introduction 1
1.1 Background 1
1.2 Problem Statement 3
1.3 Research Objectives 4
1.4 Thesis Outline 4
Chapter 2: Literature Review 6
2.1 Introduction 6
2.2 Fundamentals of Concrete Mixture 6
2.2.1 Cement (Portland Cement) 6
2.2.2 Water 6
2.2.3 Aggregates 7
2.2.4 Admixtures 7
2.2.5 SCMs 7
2. 3 Conventional Tests for Measuring Concrete Mix Water or w/cm 8
2.3.1 Slump Test 8
2.3.2 Microwave Oven Test 9
2.3.3 Phoenix Test 10
2.4 Time Domain Reflectometry (TDR) 12
2.4.1 Theoretical Background 12
2.4.2 TDR Applications in Water Content Measurement 15
Chapter 3: Research Methodology 19
3.1 Introduction 19
3.2 Material 19

3.2.1 Cement 19
3.2.2 Fly Ash 20
3.2.3 Slag 20
3.2.4 Aggregate 21
3.2.5 Water 23
3.2.6 Admixtures 23
3.3 Equipment 24
3.3.1 Humboldt Concrete Air Meter 24
3.3.2 Proceq Resipod Resistivity Meter 25
3.3.3 Campbell Scientific CR1000 Datalogger 26
3.3.4 Acclima TDR-305N Sensor 27
3.4 Mix Design Matrix 29
3.5 Mixing and Testing Procedure 30
3.5.1 Mixing and Specimen Preparation Procedure 31
3.5.2 TDR Testing Procedure 32
3.6 Data Analysis 32
3.6.1 Data Processing and Aggregation 33
3.6.2 Variable Standardization and Transformation 34
3.6.3 Polynomial Regression Model (OLS) 34
3.6.4 Measurement Error Correction (SIMEX Method) 35
3.6.5 Group-wise Modeling and Parameter Integration 36
3.6.6 Model Diagnostics 36
3.6.7 Data Analysis Summary 37
Chapter 4. Results and Discussions 39
4.1 Overview of Laboratory and Field Testing 39
4.2 TDR Results 39
4.3 Model Development and Diagnostics 42
4.3.1 Model Development 42

4.3.2 Model Diagnostics 47
4.4 Compressive Strength Results 48
4.5 Surface Resistivity Results 51
Chapter 5: Model Validation 55
5.1 Overview 55
5.2 Experimental Setup in KDOT Laboratory 55
5.3 Data Comparison 57
5.4 Discussion of Model Reliability 58
Chapter 6 Conclusions and Recommendations 60
6.1 Conclusions 60
6.2 Recommendations 60
References 62
Appendix A: Complete Mixing Matrix 66
Appendix B: Model Diagnostics Plots 69

List of Figures

Figure 1.1: Variation of concrete strength with w/c ratio..... 2

Figure 2.1: Slump test procedure (Gilson Co., 2025)..... 9

Figure 2.2: Concrete Phoenix furnace system (Gilson Co., n.d.)..... 11

Figure 2.3: (a) Schematic of a TDR device, including a pulse generator, oscilloscope, and coaxial probe inserted into soil; (b) TDR waveform of saturated sand, with travel time determined by the tangent method. (Cataldo et al., 2018)..... 14

Figure 2.4: Schematic of the TDR system used for water content monitoring in early-age concrete (adapted from Yu and Liu, 2010)..... 17

Figure 3.1: Gradation curve for mixed aggregate..... 23

Figure 3.2: Humboldt concrete air meter..... 25

Figure 3.3: Proceq Resipod resistivity meter..... 26

Figure 3.4: CR1000 Datalogger and PC150 power supply set up..... 27

Figure 3.5: Acclima TDR-305N sensor..... 27

Figure 3.6 TDR waveform in air..... 28

Figure 3.7: Measurement methods using TDR-315 sensor (Acclima, 2017)..... 29

Figure B.1: Residuals versus fitted values plot for all mixtures..... 69

Figure B.2: Williams plot for all mixtures..... 69

Figure B.3: Residuals versus fitted values plot for cement-only mixtures..... 70

Figure B.4: Williams plot for cement-only mixtures..... 70

Figure B.5: Residuals versus fitted values plot for 25% fly ash replacement mixtures..... 71

Figure B.6: Williams plot for 25% fly ash replacement mixtures..... 71

Figure B.7: Residuals versus fitted values plot for 25% GGBF replacement mixtures..... 72

Figure B.8: Williams plot for 25% GGBF replacement mixtures..... 72

List of Tables

Table 3.1: Mill Report Results for Type IL Cement Used in the Study 20
Table 3.2: Mill Report Results for GGBF Slag Cement Used in the Study 21
Table 3.3: Gradation Chart for Mixed Aggregate 22
Table 3.4: Summary of Mix Design Matrix 30
Table 4.1: Dielectric Constant of Mixtures Without SCM 40
Table 4.2: Dielectric Constant of Mixtures Containing Fly Ash 41
Table 4.3: Dielectric Constant of Mixtures Containing GGBF 42
Table 4.4: Group Mean and Group Standard Deviation 43
Table 4.5 Summary of Model Diagnostic Results 48
Table 4.6: Average Compressive Strength of Mixtures Without SCM 49
Table 4.7: Average Compressive Strength of Mixtures Containing Fly Ash 50
Table 4.8: Average Compressive Strength of Mixtures Containing GGBFS 51
Table 4.9: Average Surface Resistivity of Mixtures Without SCM. 52
Table 4.10: Average Surface Resistivity of Mixtures Containing 25% Fly-Ash 53
Table 4.11: Average Surface Resistivity of Mixtures Containing 25% GGBFS 54
Table 5.1: Summary of KDOT-1 Mixture Design 56
Table 5.2: Summary of KDOT-2 Mixture Design 56
Table 5.3: Comparison of Results from TDR and Phoenix 57
Table A.1: Mixing Matrix for 48 Mixtures 66
Table A.1: Mixing Matrix for 48 Mixtures Continue 67
Table A.1: Mixing Matrix for 48 Mixtures Continue 68

Chapter 1: Introduction

1.1 Background

Concrete is an artificial composite that consists of aggregates, such as sand, gravel, or crushed stone, and a cementitious paste. The paste is typically obtained from a mixture of Portland cement and water. It may also contain supplementary cementitious materials (SCMs), such as fly ash or ground slag, as well as chemical admixtures. Concrete is one of the most widely used building materials, supporting modern civil infrastructure, including roads, bridges, buildings, and dams. The advantages of concrete include its locally available constituents, adaptability to various shapes and sizes, and relatively high strength at a lower cost. These make concrete essential in both structural and non-structural engineering applications. The durability of concrete structures is directly related to public safety and sustainable development. Premature deterioration not only increases maintenance needs but also imposes additional economic and environmental burdens (Mehta & Monteiro, 2014).

The water-cementitious material (w/cm) ratio, a fundamental concept in concrete work, is defined as the ratio of the weight of water to the weight of cementitious materials (cement plus any SCM) in a concrete mixture. This ratio is an evolution of the water-cement (w/c) ratio, which was a ratio of the weight of water to the weight of cement. This parameter is the most important factor that controls the workability of fresh concrete and the strength and durability of hardened concrete. A lower w/cm ratio makes the fresh concrete less workable, necessitating the use of chemical admixtures, such as high-efficiency water reducers, to improve its workability. Otherwise, a higher w/cm ratio would result in lower strength, as per Abram's law, which postulated that for a given amount of consolidation, the w/c ratio is inversely proportional to the compressive strength of concrete, as shown in Figure 1.1.

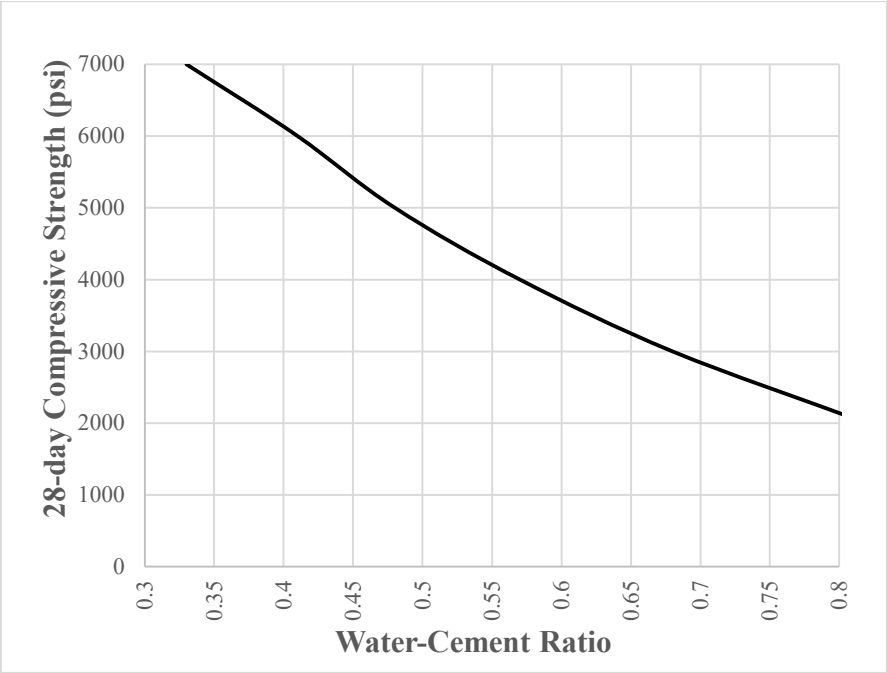

Figure 1.1: Variation of concrete strength with w/c ratio

The lower w/cm also leads to increased stiffness, reduced creep, and lower drying shrinkage. Lowering drying shrinkage reduces cracking risk. Concrete with a lower w/cm ratio will exhibit lower permeability, resulting in greater resistance to weathering and to the detrimental effects of aggressive chemicals. The lower w/cm also enhances the bond between the concrete and the embedded steel reinforcement (Kosmatka et al., 2011).

The w/c or w/cm is typically between 0.35 and 0.65 for most structural concrete. Studies have shown that when the w/c or w/cm increases from 0.4 to 0.6, the compressive strength decreases by approximately 35% (Mindess et al., 2003). Moreover, the w/cm ratio controls the durability of concrete. A lower w/cm ratio results in lower concrete permeability, reducing oxygen and chloride ion migration and helping guard against the corrosion of reinforcing steel. This, in turn, results in a higher service life for concrete. Thus, accurate control of the w/cm ratio is crucial for both the early performance and long-term durability of concrete structures, such as bridge decks. However, there is currently no fast, reliable, and non-destructive method for determining the w/cm ratio of fresh concrete at the job site. Additionally, the slump test, an empirical test that measures the response of fresh concrete to standard manipulations, is commonly used to assess concrete

workability or the w/cm ratio indirectly. The use of chemical admixtures makes this test even less reliable.

Modern moisture measurement technology may offer a solution to this problem. Time-domain reflectometry (TDR) measures the dielectric constant by tracking the velocity of high-frequency signals as they propagate through a medium. Since the dielectric constant of water is about 80, which is significantly higher than that of soil particles (2 to 7) or air (1), TDR has been widely used to estimate soil moisture content (Topp et al., 1980). In recent years, researchers have explored the application of TDR to measure moisture in cement mortar and fresh concrete. By adjusting the relationship between the dielectric constant and water content, studies have demonstrated that TDR is a feasible method for real-time moisture monitoring of materials (Cataldo et al., 2018).

1.2 Problem Statement

According to the current specifications of the Kansas Department of Transportation (KDOT), the structural concrete mix is designed to have a maximum water-to-cementitious material ratio of 0.50 and a minimum cementitious material content of 480 lb per cubic yard at an entrained air content of 6.5 ± 1.5 percent (KDOT, 2015a). The target minimum 28-day compressive strength has been outlined in the KDOT standard specification Section 401. However, recently, KDOT has observed some concrete mixes with compressive strengths below the specified values. Although the exact cause of these instances of low strength is unknown, engineers suggest that adding extra water to the concrete at the job site is primarily responsible. However, lower strength may be related to the cement, fly ash, admixtures, aggregates, or incompatibility between these materials. Thus, a method for estimating water in fresh concrete is needed. Otherwise, these non-compliant concrete mixes will continue to incur costs for KDOT due to delayed project delivery and potential poor performance if left in place. This limitation poses risks to KDOT's goals for concrete quality and durability. In recent years, KDOT has been developing performance-based quality assurance (QA) specifications for structural concrete, but has lacked the technology to rapidly and non-destructively monitor w/cm ratios in the field. Although TDR has been widely used to monitor soil water content and, in some cases, construction materials (Cataldo et al., 2018), its application to

fresh concrete has not been systematically validated; therefore, no standardized procedures are available.

1.3 Research Objectives

This study aims to address the practical challenges KDOT faces in concrete construction quality control by developing and validating a TDR-based method to determine the w/cm ratio of fresh concrete. By establishing a quantitative relationship between the dielectric constant and the w/cm ratio of fresh concrete, this study aims to provide a rapid, non-destructive, and real-time detection tool for field applications.

The specific research objectives of this study include the following:

1. To establish the correlation between the dielectric constant measured by TDR and the w/cm ratio of fresh concrete, and to propose models applicable to various concrete mixtures.
2. To systematically investigate the impact of various supplementary cementitious materials and admixtures on TDR test results and develop appropriate calibration methods.
3. To design and implement an experimental program to validate the applicability of TDR testing under laboratory and field conditions.
4. To evaluate the potential application of this method in meeting KDOT's performance-based quality assurance specifications for structural concrete and provide implementation recommendations.

1.4 Thesis Outline

This thesis is divided into six chapters. Chapter 1 introduces the research background, problem statement, and research objectives. Chapter 2 presents a literature review of the fundamentals of concrete and methods for measuring the water-to-cement (w/c) or water-to-cementitious material (w/cm) ratio. This chapter also discusses the principles and applications of TDR technology in soil and construction materials. Chapter 3 describes the research methods, including experimental

design, concrete mixtures, TDR test set-up and measurements, and data analysis methods. Chapter 4 reports the results of laboratory and field tests, focusing on analyzing the impact of different mixture components on test results and on developing models to predict w/c from TDR measurements. Chapter 5 discusses the applicability and reliability of the TDR method, as well as its potential application in KDOT's performance-based quality assurance specifications. Finally, Chapter 6 will summarize the main findings, provide practical recommendations, and outline future research.

Chapter 2: Literature Review

2.1 Introduction

This chapter reviews the fundamentals of concrete mixes, existing testing methods for measuring the water content of concrete mixtures, and related studies that provide the foundation for this research. The discussion focuses on three areas: (1) fundamentals of concrete mixtures; (2) conventional methods for evaluating the water content or the w/cm ratio of fresh concrete, and (3) application of Time Domain Reflectometry (TDR) in soil science and cementitious materials.

2.2 Fundamentals of Concrete Mixture

As mentioned earlier, a concrete mixture includes cement, water, aggregates, admixtures, and may also contain SCM as ingredients.

2.2.1 Cement (Portland Cement)

Portland cement is the most widely used type of cement in the production of concrete. It is manufactured by cintering a carefully proportioned mixture of limestone, clay, and other materials in a kiln. The resulting clinkers are then ground into a fine powder, and a small quantity of gypsum is added. When mixed with water, cement forms a paste that binds the aggregates together, holding them in place in the hardened state. There are five types of Portland cement (I through V), as defined by the American Society for Testing and Materials (ASTM), to meet the various needs of different concrete types. Type I is the most commonly used in general construction (ACI Committee 225, 2019).

2.2.2 Water

Portland cement is a hydraulic cement, meaning water is needed for hydration. During this reaction, water interacts with compounds such as tricalcium silicate (C_3S) to form calcium silicate hydrate, which provides strength (Mindess, Young, & Darwin, 2003). The w/c ratio influences concrete performance. A higher w/c ratio increases porosity and reduces durability, while a lower ratio

improves strength but may limit workability (Kosmatka et al., 2011). In practice, w/c ratio values typically range between 0.4 and 0.6 by weight (Mehta & Monteiro, 2014).

2.2.3 Aggregates

Aggregates comprise the bulk of concrete (approximately 60-75% by volume) and contribute to its strength and stability. Aggregates are typically defined as fine and coarse. Fine aggregates, such as natural sand, pass through a US No. 4 sieve (4.75 mm), while coarse aggregates, such as crushed stone or gravel, are retained on it (ASTM C33, 2018). Well-graded aggregates improve workability and minimize voids, while poorly graded ones can cause segregation or excessive paste demand (Kosmatka et al., 2011). Both bulk density and particle shape significantly influence the properties of both fresh and hardened concrete.

2.2.4 Admixtures

Most modern concrete contains chemical admixtures to modify its properties, both in the fresh and hardened states. Water reducers, often polycarboxylate-based, increase workability without adding more water (ACI Committee 212, 2010). Accelerators, such as calcium chloride, reduce the setting time and increase the hydration and strength gain rates (Mindess et al., 2003). Air-entraining admixtures, first introduced in the 1930s, increase the resistance to freeze-thaw cycles in cold climates (Kosmatka et al., 2011).

2.2.5 SCMs

Supplementary Cementitious Materials (SCMs) are inorganic materials added to concrete to enhance its properties through the pozzolanic or continuous production of cementitious gel. They are used as a partial replacement for Portland cement to enhance durability, strength, and workability. This replacement also reduces the environmental impact of cement production and its associated costs. Currently, the most common SCMs used in concrete mixtures include fly ash (Class C and Class F), ground granulated blast furnace slag (GGBFS), natural pozzolans, silica fume, calcined clay, and ground glass pozzolan (FHWA, 2016). Fly ash is a byproduct of coal combustion in power plants. The GGBFS and the silica fume are by-products, respectively, during

the production of iron and silicon/ferrosilicon alloys. Natural pozzolans consist of calcined clays, shale, and volcanic glass that are ground to a fine powder and used as substitutes for cement (FHWA, 2016).

2. 3 Conventional Tests for Measuring Concrete Mix Water or w/cm

These tests include the slump test (an indirect method), the microwave oven test, and the concrete Phoenix test. Those methods are the most common approaches for determining workability and water content. The slump test remains popular due to its simplicity; however, its correlation with the actual w/c ratio declines significantly in the presence of chemical admixtures (Neville, 2011; Mehta & Monteiro, 2014). The microwave oven test estimates water content by rapidly drying samples, and past studies have demonstrated its effectiveness. However, its accuracy depends heavily on sample uniformity and handling conditions (Mardmomen et al., 2019). More recently, the Phoenix device has been investigated as a rapid method for estimating the w/c ratio of fresh concrete. Ley and Masten (2023) reported that the Phoenix can measure the water content of fresh concrete within approximately 15 minutes, with field trials showing deviations of ±0.01 compared to design values. While the method demonstrated strong field applicability and short testing time, the authors emphasized the need for calibration to account for aggregate absorption and air content. In addition to these methods, this study also employs the air content test (KT-19), the surface resistivity test (KT-79), and the compressive strength test (KT-76). Although these do not directly measure w/c ratio, they provide complementary performance indicators that support the evaluation of both fresh and hardened concrete.

2.3.1 Slump Test

The slump test is the most commonly used method for evaluating the workability of fresh concrete. The procedure is described in KT-18 Slump of Hydraulic Cement Concrete (KDOT, 2020). In this test, concrete is placed in a standard conical mold in three layers, with each layer tamped 25 times with a rod. The tamping rod is then used to strike off the excess concrete. The cone is then steadily lifted vertically without any vibration. The difference between the mold's original height and the

collapsed concrete's height is recorded as the slump value. Due to its simplicity and the inexpensive equipment required, the slump test has been widely used in construction practices for decades.

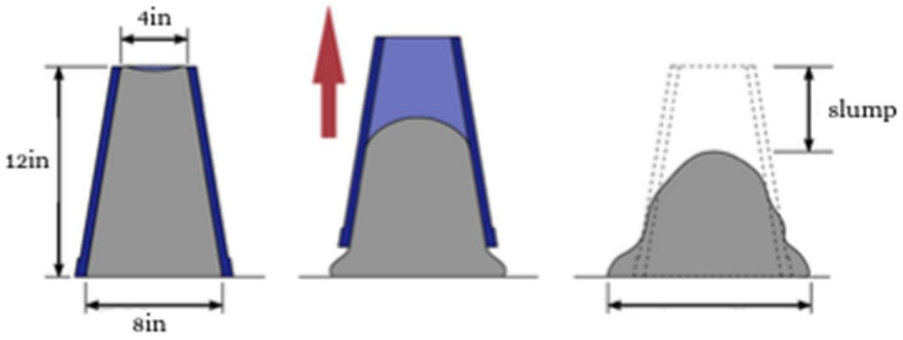

Figure 2.1: Slump test procedure (Gilson Co., 2025)

In early applications, the slump value was often considered an indirect indicator of the w/c ratio. Neville (2011) noted that, without chemical admixtures, the slump was reasonably correlated with the water content of the concrete mixture. However, with the widespread use of high-range water-reducing admixtures and plasticizers, this relationship has weakened significantly (Mehta & Monteiro, 2014). Under these conditions, concrete can achieve a high slump while maintaining a relatively low w/cm ratio, making the slump test an unreliable indicator of w/cm. The slump test is also sensitive to field conditions. The results can be influenced by mixture temperature, aggregate gradation, and operator technique (ACI Committee 211, 2002). For this reason, the test is now mainly used to evaluate workability, rather than as an indirect measure of the w/cm ratio.

2.3.2 Microwave Oven Test

The microwave oven test determines the water content of fresh concrete by drying samples with microwave radiation and measuring the associated mass loss. The method was initially developed under the Strategic Highway Research Program (SHRP) to quantify the total water content of fresh concrete delivered to construction sites (Mardmomen et al., 2019). It was later standardized as AASHTO TP23, and subsequently reclassified as AASHTO T 318, which formalized its use as a standard procedure for state transportation agencies. The method has gained popularity due to its relative simplicity and shorter testing time compared to conventional oven drying.

Despite these advantages, research has demonstrated important limitations of this method. Zheng et al. (2024) confirmed that the w/c ratio, initial moisture level, and microwave power significantly influence heating behavior and the resulting mass loss. Under higher power settings, drying tends to occur more rapidly near the sample surface than in the interior, leading to non-uniform evaporation. In addition, the microwave method measures the amount of water that can be removed under standard microwave heating conditions, and results are influenced by aggregate absorption and the portion of water that becomes chemically bound during early hydration. If mixture proportions and sampling conditions are not properly adjusted, the estimated w/c ratio may be overestimated (Mardmomen et al., 2019). Field and laboratory studies of the microwave method also pointed to systematic biases. Bechtel (2016) observed that delays between mixing and testing, as well as poor sample homogenization, led to measured water contents that deviated noticeably from the actual values. In a large-scale comparative study, Ley and Masten (2023) reported that microwave testing typically required 40 to 45 minutes per sample and used approximately 1,500 g of concrete. The results showed a variability of ±0.05 in the w/c ratio. On average, the microwave method produced values approximately 0.02 higher w/c ratio than those estimated from mix water and aggregate moisture. These findings highlight that this method introduces a consistently higher bias and suffers from limited repeatability.

Variability in equipment design for the microwave method also reduces its reliability. Differences in oven power output, frequency, and chamber geometry often lead to inconsistencies between laboratories and field sites. Larger samples often show uneven heating and localized damage, while smaller specimens improve repeatability but lack representativeness (Zheng et al., 2024).

2.3.3 Phoenix Test

The Phoenix test is a recently developed method for determining the w/cm ratio in fresh concrete. The test is similar in principle to the microwave oven method. The method relies on controlled heating of a specimen and measuring mass loss to estimate total water content, which is then combined with the cementitious material content to calculate the w/cm ratio. Unlike conventional

microwave testing, the Phoenix system utilizes a dedicated furnace, precise temperature control, and automated data logging to minimize operator error and enhance reliability (Gilson Co., n.d.).

According to the manufacturer's specifications, the Phoenix system can complete a single test in approximately 15 minutes, with a reported accuracy of ±0.01 w/cm. The standard mold capacity is 100 in^3. The testing steps include consolidating fresh concrete into a mold, weighing the specimen, transferring it into a sample pan, heating it in the Phoenix furnace, and performing a final weighing on a firebrick-insulated platform to determine mass loss. All data are automatically calculated and stored by the integrated Phoenix App (Gilson Co., n.d.).

Figure 2.2: Concrete Phoenix furnace system (Gilson Co., n.d.)

Independent evaluations support the Phoenix system's claimed performance. In a large-scale MnDOT study, Ley and Masten (2023) found that the Phoenix device consistently produced results within ±0.01 w/cm of target values in approximately 88% of field samples. The same study demonstrated that Phoenix tests required only 15 minutes compared to 40 to 45 minutes for microwave oven drying. In laboratory trials involving 144 samples, both the Phoenix and microwave methods yielded w/cm values approximately 0.02 higher than those estimated from mixing water and aggregate moisture, indicating a consistent upward bias that must be accounted for through calibration.

Researchers have also highlighted the potential of the Phoenix system within the Performance Engineered Mixtures (PEM) framework. KDOT noted that rapid and accurate determination of w/cm is essential for implementing performance-based specifications, and the

Phoenix device has emerged as a potential candidate for field deployment. However, they also emphasized the importance of standardizing calibration procedures across different mixture types to ensure reproducibility.

Despite these advantages, several limitations of the Phoenix system remain. The Phoenix system is significantly more expensive than the conventional microwave oven. Additionally, the equipment requires regular maintenance, dedicated operator training, and careful calibration to account for mixture-specific variables, such as aggregate absorption and entrained air. Also, the power requirement for running this system is substantial.

2.4 Time Domain Reflectometry (TDR)

TDR has been extensively validated in soil science as a tool for measuring soil water content based on dielectric properties (Topp et al., 1980). A few researchers have since extended this approach to cementitious materials. Berini et al. (1997) demonstrated its feasibility in mortar and concrete, noting that conductivity and mixture composition influenced the results. Cataldo et al. (2018) applied TDR under field conditions and confirmed its potential for real-time, nondestructive measurements, though calibration remained essential. These findings suggest that electromagnetic methods, including TDR, can provide a more accurate, field-ready approach to measuring the w/c ratio in fresh concrete when proper calibration and process control are implemented.

2.4.1 Theoretical Background

Time Domain Reflectometry (TDR) is a non-destructive technique that determines water content by exploiting the relationship between electromagnetic wave propagation and a material's dielectric properties. The fundamental concept is that the velocity of an electromagnetic pulse traveling through a medium is directly related to the medium’s apparent dielectric constant. Since water has a dielectric constant of approximately 78.3 at 77°F, which is significantly higher than that of aggregate, cement paste (typically 4 to 10), or air (1), variations in water content have a substantial influence on the overall dielectric behavior of the mixture (Robinson et al., 2003).

The relationship between the wave velocity and the dielectric constant is expressed as:

$$v = \frac{c}{\sqrt{K_a}} \tag{2.1}$$

Where v is the wave velocity in the medium, c is the speed of light in a vacuum, and K_a is the medium's apparent dielectric constant.

TDR obtains K_a by recording the round-travel time of the pulse along the probe of effective length:

$$K_a = \left(\frac{ct}{2L}\right)^2 \tag{2.2}$$

where t is the two-way travel time of the pulse, and L is the effective probe length.

By analyzing the reflectogram, the waveforms produced by impedance discontinuities at the probe interface and the tip can be used to identify and calculate the start and end reflection points with high precision (Cataldo et al., 2018).

Figure 2.4 represents a schematic of a TDR setup and a typical waveform. The device consists of a pulse generator, an oscilloscope, and a coaxial probe inserted into the test material. The waveform illustrates the reflection coefficient as a function of time. The sharp rise at the beginning corresponds to the air–probe interface, while the second inflection point marks the reflection at the probe tip. The distance between these points determines the travel time of the pulse, which can then be used in Eq. (2.2) to calculate the apparent dielectric constant. The tangent method is often applied to accurately determine the start and end points of the reflection curve, especially in saturated or highly conductive materials.

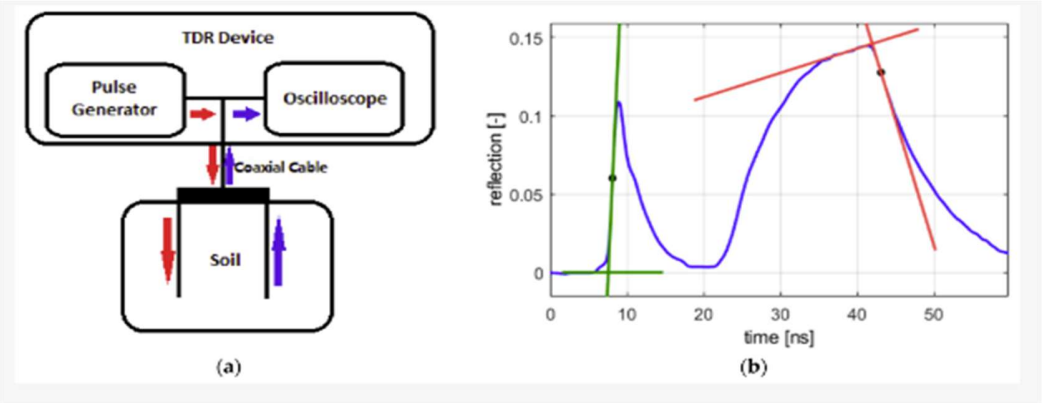

Figure 2.3: (a) Schematic of a TDR device, including a pulse generator, oscilloscope, and coaxial probe inserted into soil; (b) TDR waveform of saturated sand, with travel time determined by the tangent method. (Cataldo et al., 2018).

The sensitivity of TDR arises from the significant dielectric contrast between water, air, and solid mineral phases. Because of this disparity, even slight variations in water content produce detectable changes in the apparent dielectric constant. In practice, as water content increases, the appropriate pulse travel time and the reflectogram endpoint shift toward a larger apparent distance, indicating a higher dielectric constant.

In the theoretical framework of TDR, the propagation of electromagnetic pulses through a medium is governed not only by the bulk water content but also by the medium's ionic concentration, pore geometry, and thermal conditions. These factors collectively influence both the signal's velocity and attenuation by altering the system's effective dielectric properties (Cataldo et al., 2018).

The dielectric constant measured by TDR represents an integrated "effective value" of a heterogeneous medium, as water, air, and solid phases are spatially distributed in a non-uniform manner (Cataldo et al., 2018). Local variations in the electric field arising from this heterogeneity result in a composite response rather than reflecting the contribution of any individual phase (Robinson et al., 2003; Cataldo et al., 2018). This characteristic explains why identical changes in water content can produce distinct waveform responses when the medium's internal structure differs.

Temperature also plays a critical role in determining dielectric behavior. The dielectric constant of pure water decreases with increasing temperature, ranging from approximately 78.45 at 77°F to lower values at higher temperatures (Krishnamoorthy et al., 2021). Without proper

temperature correction, this variation can introduce systematic deviations in estimating the apparent dielectric constant, thus affecting the accuracy of water content determination (Robinson et al., 2003).

Probe geometry further affects the measurement process. The adequate sampling volume is primarily determined by probe length, while probe diameter and spacing influence the electric field distribution and sensitivity. Interactions between the probe and the surrounding phases may lead to localized perturbations in the dielectric field, resulting in small, irregular reflections in the TDR waveform (Berini et al., 1997).

2.4.2 TDR Applications in Water Content Measurement

Topp's equation is one of the most widely used empirical models in TDR applications. It was first proposed by Topp et al. (1980), who conducted systematic experiments on soils of varying texture to measure the relationship between the apparent dielectric constant and the volumetric water content. Through regression analysis, they derived a generally applicable, third-order polynomial equation to estimate the volumetric water content based on the measured apparent dielectric constant (Topp et al., 1980):

$$\theta_v = -5.3 \times 10^{-2} + 2.92 \times 10^{-2} K_a - 5.5 \times 10^{-4} K_a^2 + 4.3 \times 10^{-6} K_a^3 \quad (2.3)$$

where θ_v is the volumetric water content of soil and K_a is the apparent dielectric constant measured by TDR.

Compared to earlier approaches that relied on soil-specific calibration curves, this equation provides generalization and computational simplicity. As a result, it has been widely adopted as the standard relationship for converting TDR measurements into volumetric water content (Robinson et al., 2003). Over the past few decades, this equation has shown relatively high accuracy for most soil types. However, because it is empirical, Topp's equation also has certain limitations. For example, it does not account for the influence of electrical conductivity, temperature, or highly saline environments on dielectric properties, which may cause systematic deviations under such conditions (Robinson et al., 2003). Additionally, differences in soil texture

and bulk density can also impact the correlation between the apparent dielectric constant and water content. Therefore, although Topp's equation is highly universal, subsequent studies have emphasized the need for calibration adjustments for specific materials to ensure accurate measurements.

In addition to Topp's equation, another common approach in TDR applications is to establish material-specific empirical calibration curves that describe the relationship between the dielectric constant and volumetric water content. The procedure involves conducting measurements at a series of known water contents (θ_v), obtaining the corresponding dielectric constant K_a, and then fitting the paired data with a polynomial model. A third-order polynomial has often been found suitable, expressed as:

$$\theta_v = B_0 + B_1 K_a + B_2 K_a^2 + B_3 K_a^3 \tag{2.4}$$

where B_0, B_1, B_2, and B_3 are regression coefficients.

Cataldo et al. (2018) conducted systematic experiments on a variety of materials, including sand, bentonite, and cement-based mortars, and confirmed the suitability of this third-order polynomial model. Their results showed that, compared with linear or quadratic regressions, the cubic formulation provided a better fit to the nonlinear relationship between the dielectric constant and the volumetric water content, particularly at higher water contents. Moreover, they found that different materials exhibited distinct dielectric responses even at the same water content, reflecting the influence of composition, pore structure, and electrical conductivity.

In cementitious materials, TDR has shifted from theoretical exploration to practical validation. Berini et al. (1997) first noted that the universal Topp equation, initially developed for soils, is not directly applicable to concrete, as the electrical conductivity and aggregate composition of the mixture significantly affect the measured dielectric constant, leading to systematic deviations. Yu and Liu (2010) developed a TDR-based testing system specifically designed to monitor the early-age properties of concrete. Figure 2.5 shows the schematic of the system. It consists of a TDR pulse generator, nails of different lengths acting as probes, and a datalogger unit. This setup allows real-time monitoring of the dielectric constant of concrete

samples and their correlation with free water content. Experimental results demonstrated that TDR-based measurements of free water were in good agreement with the oven-drying method, with correlation coefficients (R^2) exceeding 0.90, and water content measurement errors generally within ±0.5%. In addition, TDR effectively captured moisture loss and changes in pore solution during early hydration, and the TDR waveforms obtained were highly consistent with those from standard methods.

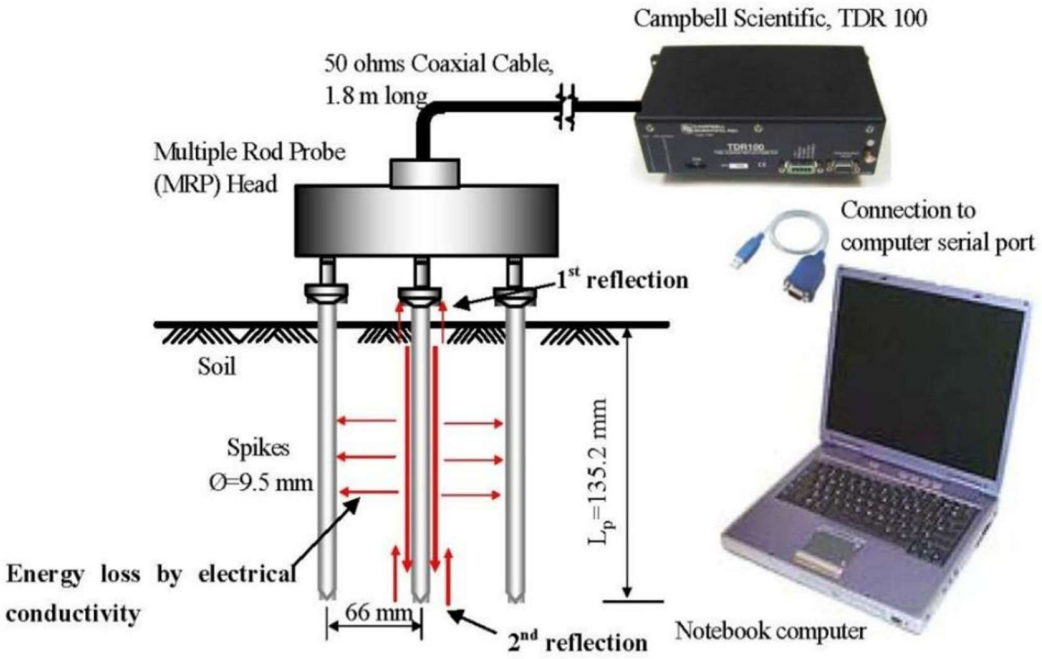

Figure 2.4: Schematic of the TDR system used for water content monitoring in early-age concrete (adapted from Yu and Liu, 2010).

In recent years, research has further expanded the application of TDR in concrete. For example, Ojala and Punkki (2024) applied TDR to automatically determine the water–cement ratio of fresh concrete, reporting a high correlation with reference methods ($R^2 \approx 0.858$). They also noted that variations in air content may introduce measurement errors. Saha et al. (2020) employed TDR to monitor the hydration process of cement paste with antifreeze admixtures under low-temperature conditions, demonstrating the feasibility of this technique in extreme construction

environments. Issa et al. (2022) also demonstrated that TDR is responsive to changes in the electrical properties of roller-compacted concrete, providing further evidence of its applicability in various concrete types.

In summary, the prevailing literature demonstrates that while traditional methods, such as the slump, microwave oven, and Phoenix tests, remain standard tools for assessing the w/c ratio, they face inherent challenges in terms of accuracy, speed, and adaptability to field conditions. TDR, on the other hand, has emerged as a promising alternative, grounded in dielectric theory and extensively validated in soils. Research has shown that TDR can capture variations in water content, hydration dynamics, and their mixtures. However, several unresolved issues, including the effects of air content, ionic conductivity, and material heterogeneity, still limit its widespread application in practice. Overall, the literature highlights TDR's potential as a rapid and non-destructive technique in cementitious systems.

Chapter 3: Research Methodology

3.1 Introduction

The limitations of conventional methods for determining the w/cm ratio in fresh concrete have been outlined earlier. TDR is promising for soils and cementitious concrete materials. However, this method has not yet been explored and validated for the concrete mixtures in Kansas. This chapter presents the experimental methodology and technical framework adopted in this study to verify the applicability of TDR in fresh concrete.

In this chapter, the primary materials, experimental tools, and equipment used in this study are first introduced. Next, the procedures for specimen preparation and the experimental design are described. This is followed by a detailed discussion of the conventional testing methods and the TDR testing procedures followed in this study. Finally, the approaches to data collection and analysis are explained, including how the results obtained from TDR were compared with those from conventional methods to evaluate consistency. Through this framework, the chapter provides the technical foundation necessary for discussing experimental results.

3.2 Material

All concrete materials used in this study were sourced from suppliers prequalified by KDOT, ensuring that the experimental/designed mixes reflect actual practice in Kansas. The materials include cement, fly ash, slag cement, fine aggregate, coarse aggregate, and admixtures. The water used in the concrete mixture was supplied by the City of Manhattan, an accepted municipal source.

3.2.1 Cement

The cement used was Type IL (Portland-Limestone) Cement, manufactured by Buzzi Unicem USA at the Cape Girardeau facility. Type IL cement is a type of blended hydraulic cement made with incorporating up to 15% finely ground limestone in ASTM Type I cement. The average chemical and physical compositions of the cement, shown in Table 3.1, met the requirements of ASTM C595. These values also met the technical requirements of cement for KDOT structural and paving concrete.

Table 3.1: Mill Report Results for Type IL Cement Used in the Study

Property		Spec. Limit	Reported Value
SO_3 (%)		3.0 max	2.7
Loss on Ignition (%)		10 max	5.2
CO2 (%)		None	4.2
Limestone (%)		15.0 max	11.6
CaCO3 in Limestone (%)		70 min	84
Na_2O Equivalent (%)		None	0.47
Air Content of Mortar (%)		12 max	7.4
Blaine Fineness (m2/kg)		None	430
Passing #325 Sieve (%)		None	91.6
Autoclave Expansion (%)		0.80 max	0.1
Compressive Strength (psi)	One day	None	2160
	Three days	1890 min	3880
	Seven days	2900 min	4820
	28 days	3620 min	6320
Time of Setting (minutes)		45–420	115
Specific Gravity		None	3.13
Heat of Hydration (3-day) - cal/g		None	69.7
Heat of Hydration (7-day) - cal/g		None	83.1

3.2.2 Fly Ash

In addition to cement, this study also utilized low-sulfate Class C fly ash sourced from the Jeffries Power Plant in northeast Kansas and supplied by Eco Material Technologies in South Jordan, Utah. This material is a byproduct of sub-bituminous coal combustion for power generation and is classified under ASTM C618. It possesses pozzolanic and self-cementitious properties. Test data indicated that its specific gravity is approximately 2.60, SO_3 content is less than 5%, loss on ignition (LOI) is below 2%, and fineness (45 μm sieve residue) is about 20%, all of which met the required specifications.

3.2.3 Slag

In addition to cement and fly ash, a Grade 100 Ground Granulated Blast Furnace Slag (GGBFS) supplied by Skyway Cement Company LLC (Chicago, Ill.) was incorporated into some of the

concrete mixtures in this study. This slag cement conforms to the requirements of ASTM C989 and AASHTO M302 for use in concrete. The average chemical and physical compositions of the slag used for the study are shown in Table 3.2.

Table 3.2: Mill Report Results for GGBF Slag Cement Used in the Study

Property		Spec Limit	Reported Value
Sulfide S (%)		2.5 max	0
SO3 (%)		None	0
Aluminum Oxide (%)		None	9.82
Chloride - CL (%)		None	0.12
Total Alkalies as Na_2O (%)		None	0.6
Residue on No. 325 Sieve (%)		20 max	0.97
Air Content (%)		12 max	4.07
Blaine Fineness (m^2/kg)		None	589
% Passing No. 325 Sieve		None	91.6
Slag Activity Index (%)	Avg. 7 Day	None	74
	Avg. 28 Day	95 min	101
Compressive Strength (psi)	7 days	None	3,248
	28 days	None	5,578

3.2.4 Aggregate

The fine aggregate was river sand supplied by Midwest Concrete Materials (MCM) from the Kaw River sand pit. Properties of the fine aggregate were determined following ASTM C128 (ASTM, 2024). The sand was immersed in water for 24 hours to ensure complete saturation. After saturation, the material was dried to a saturated surface-dry (SSD) condition and weighed. Subsequently, the aggregate was oven-dried for 24 hours, and the dry mass was recorded. The SSD bulk specific gravity was calculated by comparing the SSD and apparent masses in water, while absorption was determined from the difference between the SSD and oven-dried masses. The sand had a fineness modulus (FM) of approximately 3.23, a specific gravity of 2.62, and an absorption rate of 0.54%. The gradation met KDOT specifications for fine aggregates in concrete.

MCM also supplied the coarse aggregate. The properties of the coarse aggregate were determined in accordance with ASTM C127 (ASTM, 2024). The material was submerged in water

for 24 hours to saturate the pores, then surface moisture was removed using a towel to achieve the SSD condition. The SSD mass and the apparent mass in water were recorded, followed by oven-drying the aggregate for 24 hours to obtain the dry mass. The specific gravity of the SSD bulk was determined by comparing the SSD mass with the apparent mass, while absorption was calculated by comparing the SSD mass with the oven-dried mass. The coarse aggregate in this study had a specific gravity of 2.53 and an absorption of 4.11%.

Sieve analysis was conducted on the representative samples of fine and coarse aggregates to ensure compliance with the mixed aggregate, MA-3 specification (Division 1100 Section 1102) of KDOT (KDOT 2015b). Table 3.3 and Figure 3.1 summarize the results of the sieve analysis. Several proportioning trials were evaluated, and the selected blend consisted of 55% fine and 45% coarse aggregate, resulting in a combined gradation within the MA-3 band. The combined gradation had an FM of 4.83.

Table 3.3: Gradation Chart for Mixed Aggregate

Sieve Size (inch)	Aggregate No. 1	Aggregate No. 2	Cumulative % Retained	% Retained	Gradation Envelope	
	Sand	Coarse Aggregate			MA-3	
	55.0%	45.0%			Upper	Lower
1	0	0	0	0	0	0
¾	0	11	5	5	12	2
1/2	0	53	24	19	22	6
3/8	0	70	32	8	22	6
No. 4	4	96	45	13	22	6
No. 8	20	100	56	11	22	6
No. 16	45	100	70	14	15	6
No. 30	67	100	82	12	15	6
No. 50	89	100	94	12	15	6
No. 100	98	100	99	5	7	0
No. 200	100	100	100	1.0	2	0
Fineness Modulus	3.23	6.78	4.83	TOTAL		

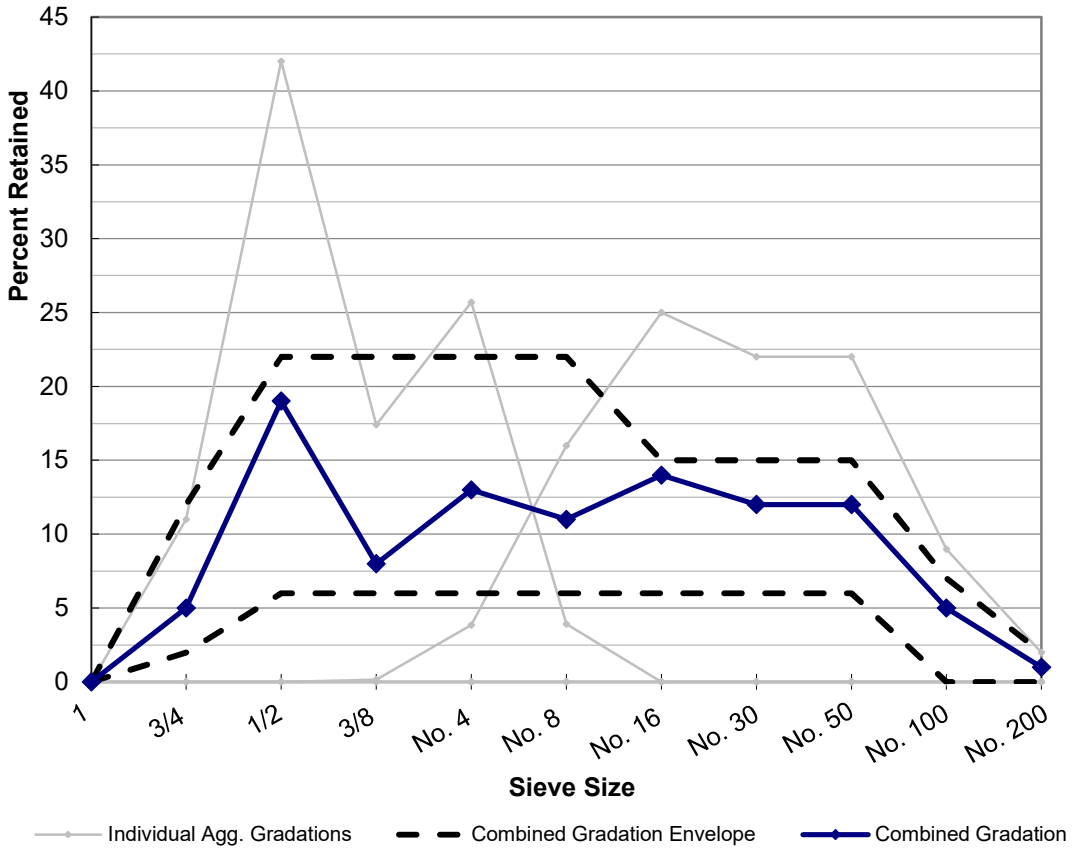

Figure 3.1: Gradation curve for mixed aggregate

The results showed that both gradation and physical properties complied with the KDOT Division 1100, Section 1102, MA-3 optimized aggregate gradation (KDOT 2015b).

3.2.5 Water

The mixing water was laboratory tap water that met the American Concrete Institute (ACI) and KDOT standards for use in concrete. The average water temperature was 68°F.

3.2.6 Admixtures

The high-range water-reducing admixture used in this study was ADVA 140M, a polycarboxylate-based admixture manufactured by GCP Applied Technologies. It was applied at a recommended dosage of 2 to 20 fl. oz per 100 lb of cement. This admixture enabled the concrete mixtures to

achieve lower water-to-cement (w/c) ratios while maintaining high workability in the fresh state and adequate strength in the hardened state.

The air-entraining admixture was Daravair 1400, manufactured by GCP Applied Technologies, which met the requirements of ASTM C260. By introducing a stable air-void system, this admixture enhances the freeze–thaw resistance of concrete and improves its long-term durability. The typical dosage ranges from 0.5 to 3 fluid ounces per 100 pounds of cement, depending on the desired entrained air level.

3.3 Equipment

All test equipment used in this study was selected to ensure compliance with the standards and to reflect the instruments commonly used in laboratory and field investigations. The equipment includes a Humboldt Concrete Air Meter, a Proceq Resipod resistivity meter, a Campbell Scientific CR1000 data logger, and an Acclima TDR-305N sensor system.

3.3.1 Humboldt Concrete Air Meter

The air content of fresh concrete in this study was measured using the Humboldt Concrete Air Meter shown in Figure 3.2, following the procedure specified in ASTM C231: Standard Test Method for Air Content of Freshly Mixed Concrete by the Pressure Method (ASTM, 2023). This pressure-type device determines the volume percentage of entrained air in freshly mixed concrete by applying a calibrated pressure to a sealed chamber containing a concrete sample.

The test procedure involves filling the measuring bowl with freshly mixed concrete in layers and consolidating each layer by rodding or vibration to ensure compaction. The cover is then clamped securely, and the chamber is filled with water to eliminate air pockets. A standard air pressure is applied, and the pressure is allowed to stabilize by releasing it into the concrete chamber. The final gauge reading indicates the air content of the mixture. This method applies to concrete with a maximum aggregate size of 2 inches and is widely used in quality control to assess compliance with freeze–thaw durability requirements (ASTM, 2023).

Figure 3.2: Humboldt concrete air meter

3.3.2 Proceq Resipod Resistivity Meter

The Proceq Resipod resistivity meter, shown in Figure 3.3, was used in this study to measure the surface electrical resistivity of hardened concrete. The device employs the four-probe Wenner method, enabling the non-destructive evaluation of the electrical properties of hardened concrete. The test procedure follows AASHTO T358: Standard Method of Test for Surface Resistivity Indication of Concrete's Ability to Resist Chloride Ion Penetration (AASHTO, 2019).

During testing, four equally spaced probes are placed on the surface of a hardened concrete cylinder. A current is applied through the two outer probes, while the potential drop is measured across the two inner probes. Using Ohm's law and a geometry correction factor, the instrument automatically calculates and displays the surface resistivity of the specimen. This method provides an indirect indication of chloride ion penetration resistance and long-term durability. This method has been increasingly adopted by KDOT and other transportation agencies as a reliable non-destructive testing approach (AASHTO, 2019).

Figure 3.3: Proceq Resipod resistivity meter

3.3.3 Campbell Scientific CR1000 Datalogger

In this study, the Campbell Scientific CR1000 data logger was used as the primary device for recording TDR data. This widely used instrument can accommodate multiple sensor channels simultaneously. Its main functions include high-precision acquisition, storage, and processing of sensor signals, as well as continuous operation over extended periods, ensuring data integrity and reliability during experiments.

In this experiment, CR1000 was used to connect and record the output signals of the Acclima TDR-305N probes. The device captured high-speed reflectogram waveforms. It calculated the apparent dielectric constant and its time-varying behavior in real-time, providing essential data for subsequent analysis of the relationship between w/cm and concrete performance. To ensure stable operation, the CR1000 was connected to a Campbell Scientific PS150 power supply (Figure 3.4), which provided a regulated input voltage and prevented signal fluctuations caused by power instability.

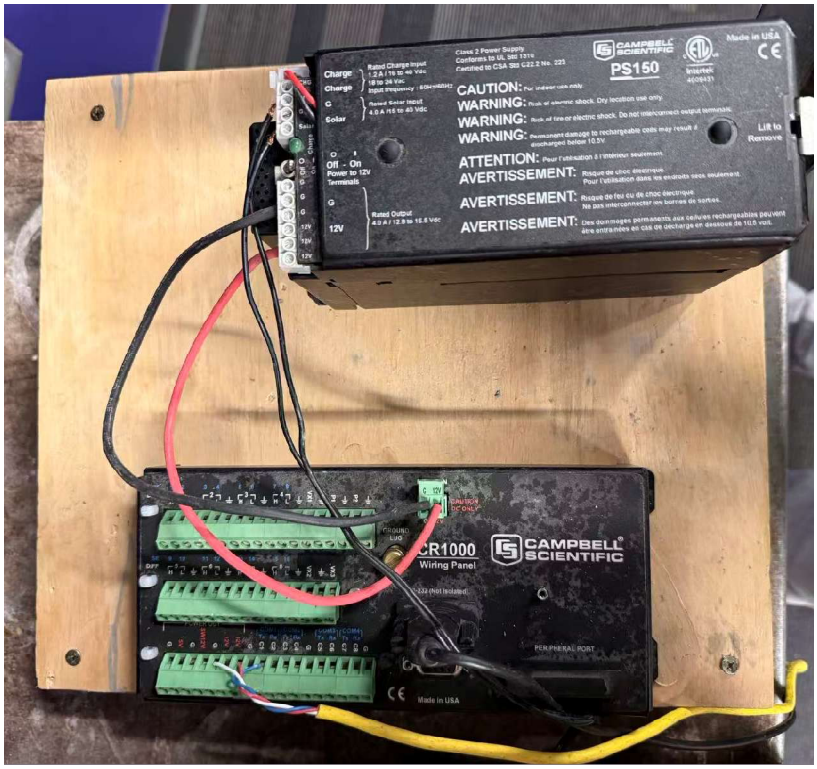

Figure 3.4: CR1000 Datalogger and PC150 power supply set up

3.3.4 Acclima TDR-305N Sensor

In this study, the Acclima TDR-305N sensor, shown in Figure 3.5, was used to measure the dielectric properties of fresh concrete.

Figure 3.5: Acclima TDR-305N sensor

The device operates by transmitting an electromagnetic pulse along the probe and recording the reflected signal to calculate the apparent dielectric constant, which indirectly reflects the water content and, in extension, the w/cm ratio of the mixture. The sensor uses the SDI-12

communication protocol and, when integrated with the CR1000 data logger, enables real-time monitoring. Unlike conventional TDR instruments, TDR-305N features a fully embedded circuit with an integrated pulse generator and probe, thereby significantly reducing instrument cost (Cataldo et al., 2018). The extremely short waveguide enables very shallow measurements, allowing the sensor to be used in environments with higher electrical conductivity.

One major challenge with this device is that a full TDR waveform contains approximately 3,000 sampling points, whereas CR1000's transmission rate supports only 3 to 4 points per second. This limitation means that recording one complete waveform would theoretically require more than 80 minutes, making real-time measurements impractical. To overcome this issue, a custom data acquisition program was developed in this study. The program sampled only every tenth point, i.e., 1, 11, 21, …, up to 3,000, resulting in 300 representative points. This reduced the acquisition time to approximately 6 minutes while maintaining waveform reliability.

The program was configured to collect a waveform every 10 minutes, with each file stored separately as "Waveform." During testing, probes had to remain stable to avoid interference from movement. As shown in Figure 3.6, the dielectric constant measured in air was approximately 1.1, which is consistent with the Acclima technical manual reference shown in Figure 3.7 (Acclima, 2017).

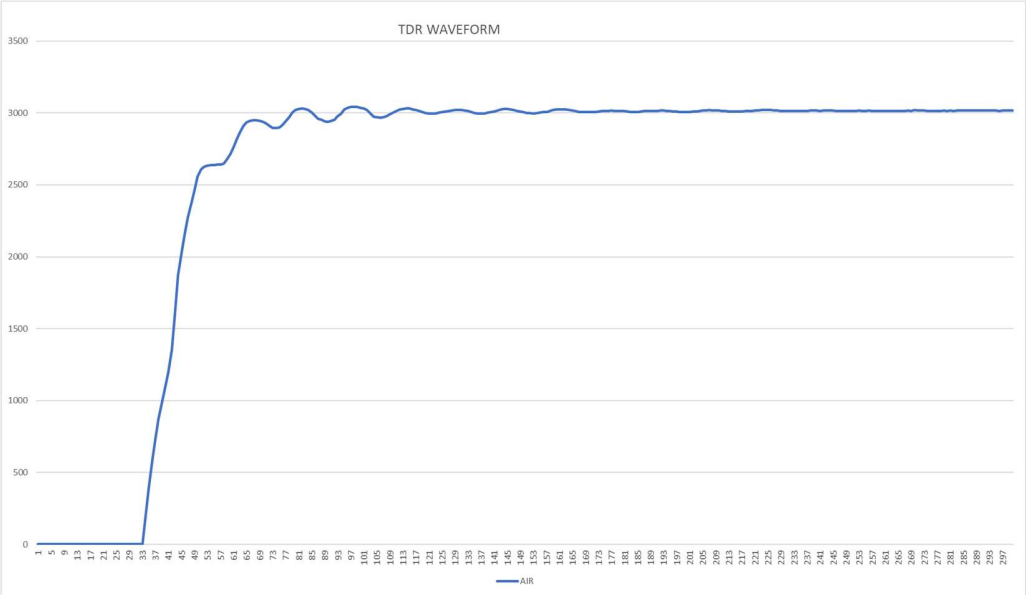

Figure 3.6 TDR waveform in air

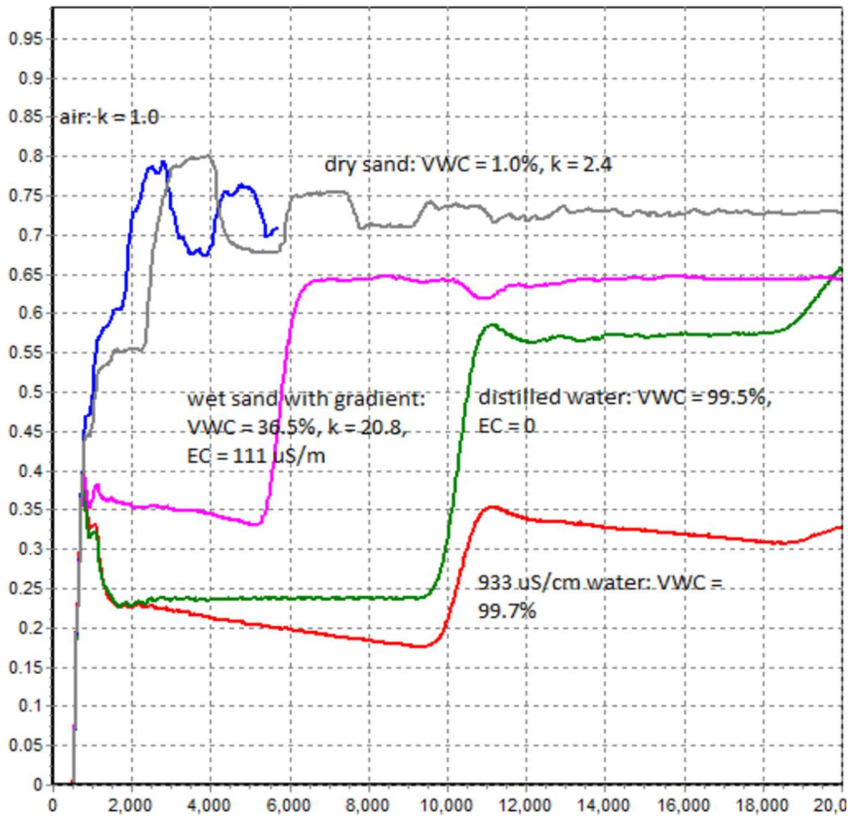

Figure 3.7: Measurement methods using TDR-315 sensor (Acclima, 2017)

3.4 Mix Design Matrix

To comprehensively investigate the influence of different variables on the dielectric properties and workability of fresh concrete, a complete factorial experimental design was adopted in this study. A mix matrix was established by combining four major factors: (1) w/cm ratio, (2) air content, (3) cementitious material content, and (4) SCM type.

First, the air content was set at two levels, 5% and 10%. The 5% level represents the typical air entrainment required for durable concrete, while 10% simulates conditions of excessive air entrainment or extreme field situations.

The w/cm ratio was chosen at two levels, 0.38 and 0.44. A w/cm ratio of 0.38 represents low w/cm mixes commonly used for high-strength or high-durability concrete. In contrast, a ratio of 0.44 is more representative of the structural concrete proportions KDOT typically uses in practice.

The cementitious material content was established at four levels: 500, 530, 560, and 590 pounds per cubic yard. These values were selected based on the typical range of cement contents in KDOT used structural concrete, covering both standard practice and mixes with higher cementitious material content for enhanced durability.

Finally, the SCM type included three categories:

1. 100% Type IL Portland cement or % SCM,
2. 25% Class C fly ash replacement (of Portland cement), and
3. 25% GGBF slag replacement (of Portland cement).

By combining these four factors, a total of 48 mix designs were generated, sequentially labeled as MX-1 to MX-48 in this study. Table 3.4 summarizes the overall design framework, presenting the significant factors and variable levels used in this study. The complete mixing matrix, including detailed combinations and corresponding IDs used in this study, is provided in Appendix A.

Table 3.4: Summary of Mix Design Matrix

Air Content	w/cm Ratio	Cementitious Material Content (lb/yd³)	SCM Type
5%	0.38	500, 530, 560, 590	0% SCM, 25% Fly Ash, 25% GGBFS
5%	0.44	500, 530, 560, 590	0% SCM, 25% Fly Ash, 25% GGBFS
10%	0.38	500, 530, 560, 590	0% SCM, 25% Fly Ash, 25% GGBFS
10%	0.44	500, 530, 560, 590	0% SCM, 25% Fly Ash, 25% GGBFS

3.5 Mixing and Testing Procedure

To ensure the reliability and repeatability of experimental data, the test procedure for fresh concrete was systematically designed and consisted of two main steps: TDR testing and conventional performance tests.

3.5.1 Mixing and Specimen Preparation Procedure

To align with KDOT field practices, this study followed a standardized mixing and preparation protocol. Coarse and fine aggregates were first oven-dried at 230°F for 24 hours to remove pore water. Their absorption capacity was then determined in accordance with ASTM C127 and ASTM C128, and the corresponding absorption water was added before mixing to achieve the SSD condition.

The detailed mixing steps were as follows:

1. Add 80% of the total mixing water into the mixer, together with the specified dosage of the air-entraining admixture (Daravair 1400) and high-range water-reducing admixture (ADVA 140M).
2. Introduce approximately 40% of the coarse aggregate and 20% of the fine aggregate, and start the mixer for preliminary blending.
3. Add all cementitious materials (cement, fly ash, or ground slag) at once, along with part of the remaining fine aggregate.
4. Add the remaining 60% of coarse aggregate and 80% of fine aggregate.
5. Add the final 20% of the mixing water to ensure the target water-to-cement ratio is achieved.
6. Mix for 3 minutes, cover and rest for 3 minutes, then continue mixing for another 2 minutes to ensure uniformity.
7. Conduct slump (KT-18) and air content (KT-19) tests immediately after mixing.
8. Cast the concrete into 4×8 in. cylindrical molds using layered consolidation. A total of 17 specimens were prepared: 12 for compressive strength testing at 7, 14, 28, and 56 days; 3 for surface resistivity testing; and 2 for hardened air-void analysis by KDOT.
9. All specimens were kept in a climate-controlled curing room (23 ± 2°C, relative humidity >95%) for 24 hours before demolding and then returned to the curing room on demolding until testing.

3.5.2 TDR Testing Procedure

To ensure representative results, the TDR testing procedure was optimized to capture both reference and multi-positional data. The detailed steps are as follows:

1. Fresh concrete was placed in a 5-gallon Poly Vinyl Chloride (PVC) bucket, filled to a depth of approximately three-fourths of the bucket (minimum 12 cm depth). The Acclima TDR-305N probe was vertically inserted into the center of the bucket, and a complete waveform was recorded as the baseline reference.
2. After the baseline waveform was collected, the CR1000 data logger program was switched to a 5-second sampling interval, allowing continuous monitoring of dielectric properties.
3. The probe was positioned sequentially at five locations: center, 0°, 90°, 180°, and 270°. At each location, measurements were recorded for 2 minutes. This approach was adopted to account for potential non-uniform moisture distribution resulting from the mixing process, thereby enhancing the representativeness of the collected data.
4. All waveform data collected during the cycle were exported to an Excel spreadsheet. Electrical conductivity and dielectric constant values were processed by excluding extreme values (maximum and minimum) and computing the average. This provided a representative parameter for the batch of fresh concrete.

By combining a central reference measurement with multi-positional sampling, this procedure ensured that both local and global variations in moisture distribution were adequately captured, thereby enhancing the reliability of TDR measurements.

3.6 Data Analysis

This section presents the procedure of instrument calibration for the TDR sensor and associated statistical data analysis. All statistical analyses and model development in this study were performed in the R statistical environment (R Core Team, 2024). The entire workflow, from raw TDR data processing to regression modeling, was executed within R using standard packages, including dplyr, readxl, and simex. This section describes the complete data analysis methodology

for establishing the quantitative relationship between the apparent dielectric constant (K_a) and the volumetric water content (θ_v) of fresh concrete mixtures. The procedure involves data aggregation, variable standardization, logit transformation, polynomial regression, and SIMEX-based measurement-error correction (Cook & Stefanski, 1994; Carroll et al., 2006), resulting in a statistically robust and physically interpretable calibration framework.

3.6.1 Data Processing and Aggregation

To minimize random fluctuations and to quantify the precision of TDR measurements, multiple readings obtained from each mixture were statistically aggregated.

The mean and standard deviation of the apparent dielectric constant for each mixture, i were computed as:

$$\overline{K_{a,i}} = \frac{1}{n_i}\sum_{j=1}^{n_i} K_{a,ij} \tag{3.1}$$

$$S_{x,i} = \sqrt{\frac{1}{n_i-1}\sum_{j=1}^{n_i}\left(K_{a,ij} - \overline{K_{a,i}}\right)^2} \tag{3.2}$$

where $\overline{K_{a,i}}$ is the mean apparent dielectric constant of the i mixture, $K_{a,ij}$ represents the individual measurement, n_i is the number of readings, and $S_{x,i}$ denotes the within-group standard deviation.

To describe the overall precision of the TDR system, the group-wise variances were pooled using a weighted formulation:

$$S_{x,\text{global}} = \sqrt{\frac{\sum_i (n_i-1)S_{x,i}^2}{\sum_i (n_i-1)}} \tag{3.3}$$

where, $S_{x,\text{global}}$ represents the global standard deviation of the measurement error, which is later used as the input parameter for the SIMEX correction.

3.6.2 Variable Standardization and Transformation

Because the magnitude of K_a differed among mixture groups, each dataset was standardized to ensure comparability and numerical stability.

$$K_{a,c} = \frac{K_a - \overline{K_a}}{s_{K_a}} \tag{3.4}$$

where $K_{a,c}$is the standardized apparent dielectric constant, K_a is raw measured dielectric constant, $\bar{K_a}$ is the group mean, and $s_{K_a}$is the standard deviation of K_a within the same mixture group.

To prepare for subsequent error correction, the global measurement error obtained from Section 3.6.1 was converted to a standardized scale using the following relationship:

$$S_{x,\text{scaled}} = \frac{S_{x,\text{global}}}{s_{K_a}} \tag{3.5}$$

where $S_{x,\text{scaled}}$ is equivalent to the measurement uncertainty of $K_{a,c}$ after normalization.

To avoid nonlinear compression near the saturation or dry limits of θ_v , a logit transformation was applied:

$$z = \ln\left(\frac{\theta_v}{1-\theta_v}\right) \tag{3.6}$$

where z is the transformed variable, mapping $\theta_v \in (0,1)$ on to the real number domain, thereby improving linearity across the full range of water contents.

The inverse transformation recovers the volumetric water content from the predicted logit value:

$$\theta_v = \frac{1}{1+\mathrm{e}^{-z}} \tag{3.7}$$

3.6.3 Polynomial Regression Model (OLS)

After variable transformation, the relationship between z and $K_{a,c}$ was modeled using a cubic polynomial to capture the nonlinear dielectric behavior of fresh concrete:

$$z = \beta_0 + \beta_1 K_{a,c} + \beta_2 K_{a,c}^2 + \beta_3 K_{a,c}^3 \tag{3.8}$$

where $\beta_0, \beta_1, \beta_2$ and β_3 are the regression coefficients.

The cubic form provides sufficient flexibility to accommodate both low- and high-moisture regions while maintaining physical interpretability consistent with the empirical Topp equation.

The model coefficients were estimated by the Ordinary Least Squares (OLS) method, minimizing the sum of squared residuals:

$$\min_{\boldsymbol{\beta}} \sum_k (z_k - \hat{z}_k(\boldsymbol{\beta}))^2 \tag{3.9}$$

The model fit was evaluated by using the coefficient of determination:

$$R^2 = 1 - \frac{\sum_k (z_k - \hat{z}_k)^2}{\sum_k (z_k - \bar{z})^2} \tag{3.10}$$

where $\hat{z}_k$ is the predicted value, $\bar{z}$ is the mean of the observed data and R^2 is the coefficient of determination. A higher R^2 indicates stronger agreement between model predictions and experimental observations.

3.6.4 Measurement Error Correction (SIMEX Method)

Since the measurement uncertainty in TDR readings tends to attenuate the regression slope and bias model coefficients, the SIMEX method (Cook & Stefanski, 1994; Carroll et al., 2006) was adopted to correct for this systematic effect.

The core idea of SIMEX is to amplify the noise level artificially, observe how the estimated coefficients vary with the magnitude of the simulated error, and then extrapolate the trend to the "no-error" condition ($\lambda = -1$).

The procedure consists of three significant steps:

1. Noise injection: Random noise is progressively added to the predictor $K_{a,c}$, with amplification factors $\lambda = 0.5, 1.0, 1.5$ and 2.0.
2. Repeated fitting: For each noise level λ, an OLS regression is performed, producing a sequence of coefficient estimates, $\hat{\beta}(\lambda)$.
3. Extrapolation: The relationship between $\hat{\beta}(\lambda)$ and λ is fitted by a quadratic polynomial, which is then extrapolated to $\lambda = -1$ to obtain the bias-corrected actual coefficient:

Through SIMEX correction, the physical consistency of regression coefficients is significantly improved. In particular, the fitted curve better matches the experimental observations in the high-moisture region, effectively mitigating the systematic underestimation caused by measurement noise.

3.6.5 Group-wise Modeling and Parameter Integration

To investigate the effect of different binder systems, all mixtures were categorized into four groups:

1. All datasets.
2. Cement-only mixtures dataset.
3. Fly ash mixtures dataset.
4. GGBFS mixtures dataset.

Each group was processed independently following the same workflow (standardization → OLS → SIMEX).

3.6.6 Model Diagnostics

To verify the regression models, the Breusch-Pagan (BP) test and two diagnostic plots, the residuals vs. fitted plot and the Williams plot, were generated using built-in functions in R.

The BP test is used to detect the presence of heteroskedasticity in a linear regression model. Heteroskedasticity refers to the variance of the model's error being non-constant, changing systematically with independent variables or fitted values, which renders the estimated standard errors and significance tests unreliable (Wooldridge, 2019). The BP test performs an auxiliary regression in which the squared residuals are regressed on the explanatory variables to check whether the error variance is statistically related to them (Breusch & Pagan, 1979). If the squared residuals show a significant relationship with the explanatory variables, that would indicate error variance is not constant and heteroskedasticity exists. Statistically, the BP test used a Lagrange Multiplier (LM) and evaluated its significance based on the chi-square distribution. When the p-value is smaller than the chosen significance level (typically 0.05), the null hypothesis of homoskedasticity is rejected, which suggests that heteroskedasticity exists; otherwise, the variance is considered stable (Greene, 2018).

In addition to the BP test, visual diagnostics were conducted using the residuals versus fitted plot and the Williams plot to evaluate the model's performance further. The residuals vs fitted plot visually examines whether residuals are randomly distributed along the fitted values, helping detect potential nonlinearity, unequal variance, or systematic bias in the regression model. Ideally, the residuals should scatter randomly around zero without any distinct pattern, indicating that the model satisfies the assumptions of homoskedasticity and linearity. Conversely, a visible funnel shape or curvature suggests the possibility of heteroskedasticity or model misspecification (Montgomery et al., 2021). The Williams plot combines standardized residuals and leverage values to identify outliers and high-leverage observations that could disproportionately influence the regression coefficients (Williams, 1959). The leverage value h_i measures each data point's influence within the predictor space, while the standardized residual reflects its deviation from the fitted model. Observations with standardized residuals exceeding ±3σ are typically considered as outliers, and those with leverage values above the empirical threshold h^* are considered high-leverage points (Montgomery et al., 2021).

3.6.7 Data Analysis Summary

This section developed an R-based workflow to establish a quantitative relationship between the apparent dielectric constant (K_a) and volumetric water content (θ_v) of fresh concrete. The following steps were followed:

1. Raw TDR data from all mixtures were aggregated and processed to estimate both group and global measurement uncertainties.
2. Each dataset was standardized to remove scale effects, and the response variable θ_v was transformed using a logit function to improve model linearity.
3. A cubic polynomial regression model was then fitted using OLS to capture the nonlinear dielectric behavior across different binder systems.
4. The SIMEX method was applied to correct slope attenuation caused by measurement errors, followed by parameter pooling to integrate results from cement-only, fly ash, and GGBFS mixtures.

5. Finally, the model was verified by using the BP test, the residuals vs fitted plot, and the Williams plot.

Chapter 4. Results and Discussions

4.1 Overview of Laboratory and Field Testing

This chapter presents the results of all tests performed for this study. The overall experimental plan was executed at the Concrete Laboratory of Kansas State University and at the Materials and Research Center of the Kansas Department of Transportation (KDOT) in Topeka. The tests included slump, air content, and TDR measurements on fresh concrete, as well as compressive strength and surface electrical resistivity of hardened concrete.

All concrete mixtures followed the mix design and batching procedures outlined in Chapter 3. The specimens were prepared using the materials mentioned in Chapter 3. Hardened concrete specimens were tested after controlled curing consistent with KDOT standard procedures KT-76 (KDOT, 2015) for compressive strength and KT-79 (KDOT, 2015) for surface resistivity. The TDR tests were performed immediately after mixing to capture the dielectric behavior of the fresh mix and to develop calibration models linking the apparent dielectric constant (K_a) to volumetric water content (θ_v). Together, these datasets were used to analyze the effects of mixture parameters on the dielectric response of fresh concrete, strength development, and electrical resistivity, and to validate the predictive capability of the proposed TDR-based w/cm ratio measurement framework.

4.2 TDR Results

This section presents the TDR test results obtained from 48 concrete mixtures. The test procedures followed the method described in Chapter 3. Multiple measurements were done for each mixture, and the minimum, maximum, and average apparent dielectric constant values (K_a) were reported as representative results. Table 4.1 tabulates the results for the mixtures without SCM.

Table 4.1: Dielectric Constant of Mixtures Without SCM

Mix ID	Dielectric Constant		
	Min.	Max.	Avg.
MX-1	10.1	15.2	14.00
MX-2	10.1	18.8	16.02
MX-3	17.6	22.6	20.44
MX-4	18.7	23.0	21.88
MX-13	19.1	20.7	19.85
MX-14	19.5	22.5	20.90
MX-15	20.4	23.2	22.45
MX-16	22.8	24.4	23.75
MX-25	14.1	18.3	16.39
MX-26	15.2	19.7	18.47
MX-27	16.7	20.4	19.54
MX-28	18.6	21.3	20.75
MX-37	19.6	20.2	19.91
MX-38	19.8	22.4	21.66
MX-39	22.0	23.1	22.43
MX-40	23.7	24.5	24.08

The results in Table 4.1 show that the average apparent dielectric constant ranged from 10 to 24, with most values between 14 and 22. For mixtures of similar w/cm ratios (e.g., MX-1, MX-2, MX-3, and MX-4), an increase in cement content led to a higher mixing water demand and, consequently, a higher volumetric water content, resulting in a gradual increase in the measured dielectric constant. For mixtures with comparable cement content (e.g., MX-1 and MX-13), a higher w/cm ratio yielded higher dielectric constants. Overall, the observed trend is consistent with the governing effect of the water phase on the dielectric behavior of concrete: as the proportion of free water increases, the TDR signal propagation velocity decreases, leading to higher values of K_a. Additionally, the range between the maximum and minimum values reflects the degree of moisture distribution within each mixture. In extreme cases, such as MX-1, the lowest w/cm ratio and cement content resulted in unavoidable nonuniformity in moisture distribution, leading to a broader spread in the measured dielectric constant values.

Table 4.2 summarizes the apparent dielectric constant results for mixtures containing 25% fly ash. The measured values ranged from 10 to 25, with most averages between 14 and 24. Compared with the no-SCM mixtures, the fly ash mixtures generally exhibited slightly lower

dielectric constants at the same w/cm ratio. However, the overall variation followed a similar trend to that of the only cement mixtures, and no significant difference was observed between the two groups.

Table 4.2: Dielectric Constant of Mixtures Containing Fly Ash

Mix ID	Dielectric Constant		
	Min.	Max.	Avg.
MX-5	10.4	18.2	14.53
MX-6	14.2	19.2	16.85
MX-7	17.4	22.8	20.22
MX-8	17.1	21.8	20.14
MX-17	14.5	20.5	17.27
MX-18	15.5	23.6	20.68
MX-19	17.7	21.8	20.95
MX-20	22.4	24.8	23.25
MX-29	18.2	18.2	18.61
MX-30	18.3	20.0	19.29
MX-31	19.7	20.8	20.46
MX-32	20.9	21.9	21.39
MX-41	20.4	21.3	21.00
MX-42	21.3	22.1	21.76
MX-43	21.8	23.3	22.58
MX-44	22.7	25.6	24.09

Table 4.3 summarizes the apparent dielectric constant results for mixtures containing 25% GGBFS. The measured values ranged from 10 to 23, with most averages between 14 and 22. Compared with the other two groups, the GGBFS mixtures exhibited different trends in some cases. In the mixtures with a 0.38 w/cm ratio (MX-9, MX-10, MX-11, and MX-12), the measured dielectric constants showed an inconsistent pattern, in contrast to the steady increase observed in other mixes. This irregularity may be attributed to the intrinsic physical characteristics of GGBFS. A study conducted by Haddad and Chung (2017) reported that the addition of graphite nanoplatelets to cement significantly reduced the dielectric constant of the composite material. By analogy, it is possible that GGBFS, during the hydration process, alters or partially impedes the polarization of concrete containing GGBFS, leading to unstable dielectric constant readings in the TDR measurements.

Table 4.3: Dielectric Constant of Mixtures Containing GGBF

Mix ID	Dielectric Constant		
	Min.	Max.	Avg.
MX-9	10.1	18.9	14.44
MX-10	11.1	16.4	14.17
MX-11	12.9	18.1	14.91
MX-12	15.2	19.2	17.56
MX-21	14.4	18.9	16.89
MX-22	19.0	19.8	19.39
MX-23	18.4	21.4	20.53
MX-24	21.6	22.4	21.95
MX-33	15.3	16.7	16.08
MX-34	17.1	18.4	17.86
MX-35	17.1	18.7	18.17
MX-36	19.2	20.7	19.86
MX-45	17.0	19.2	18.83
MX-46	19.1	21.2	20.86
MX-47	21.6	23.0	22.11
MX-48	21.6	23.0	22.11

4.3 Model Development and Diagnostics

This section presents the development and validation of the relationships between the apparent dielectric constant, K_a and the volumetric water content, θ_v of fresh concrete. The goal of the modeling process is to translate the TDR measurements into a reliable predictor of the concrete water-to-cement/cementitious materials ratio (w/c or w/cm). Building on the experimental data obtained from 48 mixtures, the analysis was conducted in the R environment using a structured workflow that integrated statistical regression, variable standardization, and measurement error correction.

4.3.1 Model Development

Figures 4.1 through 4.4 present the regression models developed for the four cementitious systems based on the data analysis procedure described in Chapter 3. In each figure, the solid black line represents the fitted regression curve, the dashed gray lines indicate the 95% confidence intervals (95% CI), and the scattered points present the measured dielectric constant and volumetric water content of each mixture. The general regression model is expressed as:

$$z = \beta_0 + \beta_1 K_{a,c} + \beta_2 K_{a,c}^2 + \beta_3 K_{a,c}^3 \quad (4.1)$$

where z is transformed θ_v, and $\beta_0, \beta_1, \beta_2, \beta_3$ are the regression coefficients. The variable $K_{a,c}$ refers to the standardized apparent dielectric constant.

For the standardized apparent dielectric constant (Equation (3.4)), each group will have a different group mean, $\bar{K_a}$, and group standard deviation, s_{K_a}. Those coefficients were obtained from raw datasets of 48 mixtures, and the results are presented in Table 4.4.

Table 4.4: Group Mean and Group Standard Deviation

Mix Group	K_a	s_{K_a}
All	19.800	3.060
Cement only	20.210	3.030
Fly-Ash	19.740	2.840
GGBFs	19.470	3.210

To convert the predicted z values into actual volumetric water content θ_v, the inverse logit function is followed by equation 3.7.

Equation 4.3 and Figure 4.2 show the model developed for all concrete mixtures.

$$\text{logit}(\theta_v) = -1.7834 + 0.0855 K_{a,c} + 0.0212 K_{a,c}^2 + 0.0020 K_{a,c}^3 \quad (4.2)$$

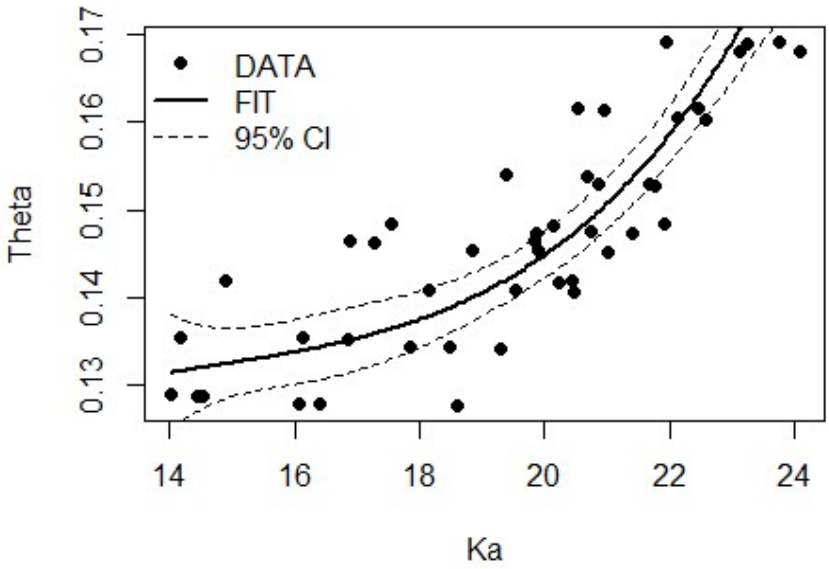

Figure 4.1: Calibration curve of volumetric water content (Theta) versus Ka for all mixtures

The model was developed based on all 48 mixtures, with a coefficient of determination, R^2 of 0.73. The overall trend shows a clear, nonlinear positive correlation between the apparent dielectric constant. $K_a$and the volumetric water content θ_v. As illustrated in Figure 4.1, the data points in the lower region (K_a=14 –18) are relatively scattered, and the confidence interval is wider, indicating variability in dielectric response among different mixtures. In contrast, as the confidence interval narrows, it suggests improved consistency of the dielectric behavior at higher moisture contents and reduced prediction uncertainty.

Overall, this model effectively represents the general trend across all mixtures, showing stable performance in the high-moisture range. However, in the mid-range water-cement ratios, minor deviations may still occur due to the influence of different cementitious systems.

The model for a mixture containing only cement is shown in Equation (4.3) and illustrated in Figure 4.2.

$$z = -1.7903 + 0.1113K_{a,c} + 0.0246K_{a,c}^2 - 0.0009K_{a,c}^3 \quad (4.3)$$

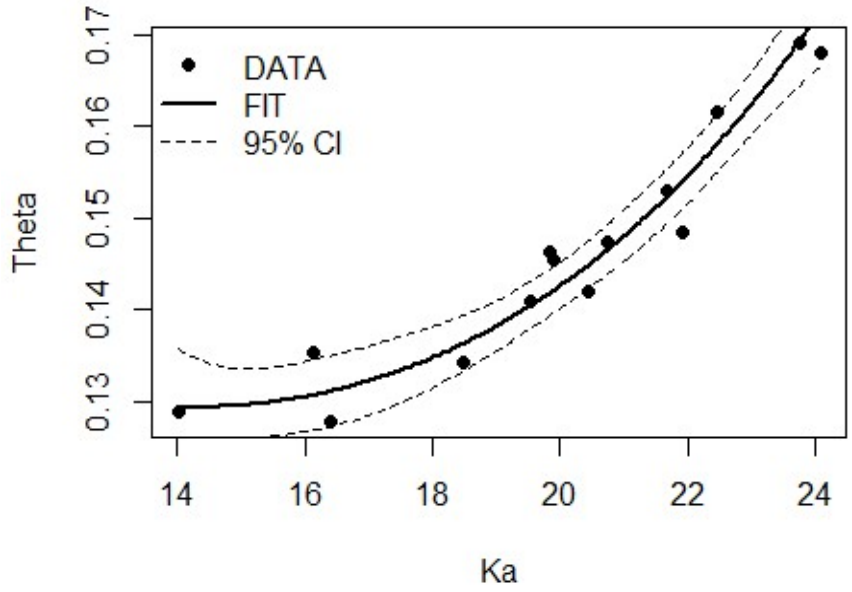

Figure 4.2: Calibration curve of volumetric water content (Theta) versus Ka for cement-only mixtures

The cement-only model achieved the highest fitting accuracy, with a coefficient of determination, R^2 of 0.94. As shown in Figure 4.2, the data points are tightly distributed, and the 95% confidence interval is the narrowest among all models, indicating a highly consistent dielectric response with minimal measurement error. The fitted curve exhibits an almost linear increase in the range of K_a of 14 to 20, suggesting that, in this system, the polarization effect is approximately proportional to the water phase ratio.

Overall, this model demonstrates strong physical consistency and stability; however, its applicability is limited to mixtures without any SCM.

Equation 4.4 and Figure 4.3 show the models for concrete mixtures containing 25% fly ash. The model has a coefficient of determination (R^2) of 0.71.

$$z = -1.7921 + 0.0770K_{a,c} + 0.0330K_{a,c}^2 + 0.0085K_{a,c}^3 \quad (4.4)$$

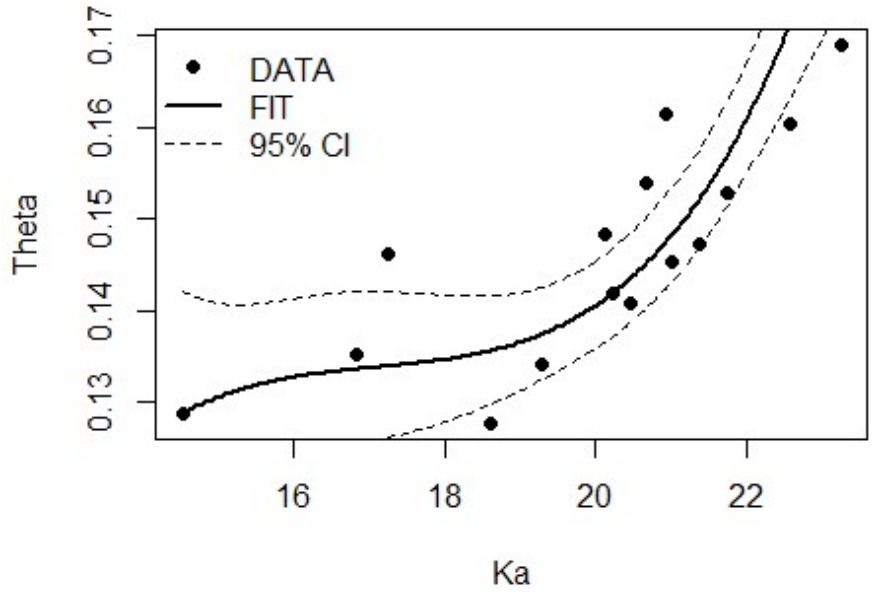

Figure 4.3: Calibration curve of volumetric water content (Theta) versus Ka for 25% fly ash replacement mixtures

As shown in Figure 4.3, the apparent dielectric constant K_a and the volumetric water content θ_v has a nonlinear positive correlation, and the data points are more scattered than in the cement-only group. The slope of the fitted curve increases slowly in the range of K_a of 13 to 16, and the curve becomes noticeably steeper when $K_a > 19$, indicating that the dielectric response is relatively weak under lower moisture conditions but gradually strengthens as the volumetric water content increases. This nonlinear behavior is possibly associated with the dispersion of fly ash.

While the model reasonably captures the overall trend, the wider confidence interval and greater residual dispersion indicate significant variability in dielectric response across various fly ash mixtures, primarily due to the instability introduced by fly ash. The equation for this model is expressed as:

Equation (4.5) and Figure 4.4 show the model for concrete mixtures containing GGBF.

$$z = -1.7721 + 0.1065K_{a,c} + 0.0162K_{a,c}^2 - 0.0093K_{a,c}^3 \quad (4.5)$$

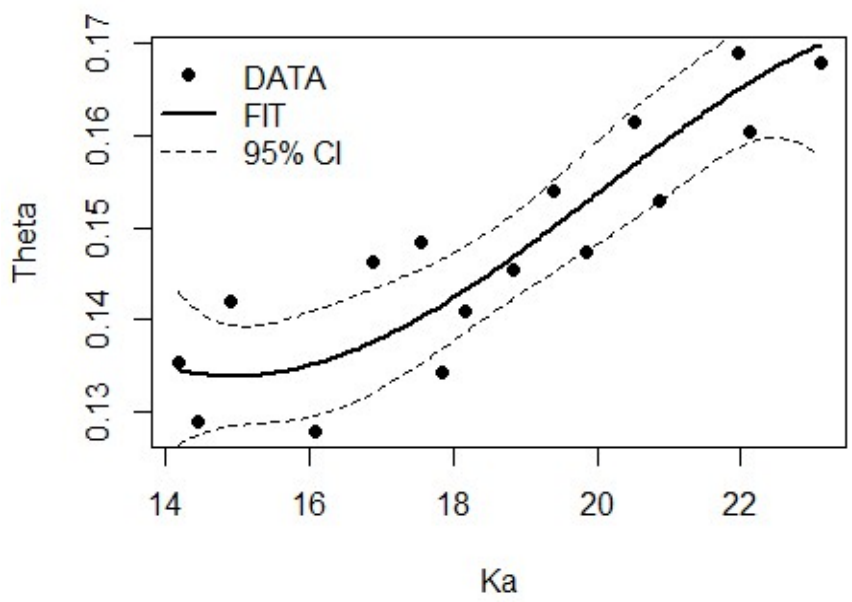

Figure 4.4: Calibration curve of volumetric water content (Theta) versus Ka for 25% GGBF replacement mixtures

The model for mixtures containing 25% ground granulated blast-furnace slag (GGBFS) achieved a coefficient of determination of $R^2 = 0.79$. As shown in Figure 4.4, the fitted curve increases steadily in the range of K_a of 14 to 17 and slightly declines when $K_a > 18$, exhibiting a mild saturation effect in which the increase in dielectric constant slows at higher moisture contents.

Due to the influence of GGBFS, the dielectric response of this system appears less stable, leading to reduced model reliability. Overall, the model captures the primary relationship between $K_a$and θ_v. However, its predictive accuracy is affected by the material properties inherent to slag-blended systems.

4.3.2 Model Diagnostics

This section presents the model diagnostics results for the developed TDR calibration models. Table 4.5 summarizes the critical information obtained from the BP test and William's plot.

Table 4.5 Summary of Model Diagnostic Results

Mix Group	BP p-value	Leverage Threshold h*	Max Leverage, h	Standardized Residuals exceed ±3σ
All	0.1782	0.2667	0.3987	0.0000
Cement	0.7597	0.8571	0.9459	0.0000
Fly Ash	0.3473	0.8000	0.9778	0.0000
GGBFS	0.0545	0.7500	0.7514	0.0000

The Breusch–Pagan (BP) test results indicated that all models satisfied the homoskedasticity assumption, with p-values above 0.05. Although the GGBF group showed a p-value close to the significance threshold, it did not exceed the 0.05 level, suggesting only mild variance fluctuation that does not compromise model stability.

The residuals vs. fitted plots showed that the residuals for all groups were randomly distributed around zero, without any visible trend or funnel pattern, confirming that the models met the assumptions of linearity and constant variance.

Further analysis using the Williams plots, which combine standardized residuals and leverage values, revealed that all standardized residuals were within ±3σ, indicating the absence of outliers. Although the maximum leverage values in some groups slightly exceeded the theoretical threshold h^*, these data points did not deviate significantly from the overall trend and had no detrimental influence on the fitted regression coefficients.

All related diagnostic plots, including the BP test results, residuals vs fitted plots, and Williams plots, are provided in Appendix B for reference. Overall, the diagnostics confirmed that the regression models were statistically stable and well specified, with no influential observations or systematic errors, demonstrating the reliability and consistency of the TDR calibration models.

4.4 Compressive Strength Results

This section presents the results of compressive strength testing, as outlined in KT-76 (KDOT, 2018), which specifies the Test for Compressive Strength of Cylindrical Concrete Specimens. All specimens were prepared following the mixture proportions and batching procedures described in Chapter 3 and were cured under standard conditions (relative humidity ≥ 95%, temperature = 23 ± 2 °C). For each mixture (MX-1 through MX-48), three cylindrical specimens with a diameter of

4 in. and a height of 8 in. were cast and tested at curing ages of 7, 14, 28, and 56 days. Testing was conducted using a Forney compression testing machine with a controlled loading rate of 35 ± 7 psi/s. The reported strength values, tabulated in Table 4.1, represent the average of three samples based on the maximum applied load, expressed in pounds. The reported strength values represent the average of three samples based on the maximum applied load, expressed in pounds per square inch (psi).

Table 4.6: Average Compressive Strength of Mixtures Without SCM

Mix ID	Compressive Strength (psi)			
	7 Day	14 Day	28 Day	56 Day
MX-1	2,880	3,320	3,120	3,320
MX-2	5,070	3,980	5,100	5,460
MX-3	5,280	5,980	6,160	6,260
MX-4	5,450	6,050	6,670	6,890
MX-13	4,730	5,360	5,240	5,670
MX-14	4,980	5,430	5,910	6,350
MX-15	4,490	5,210	5,960	5,970
MX-16	5,020	5,570	6,180	6,400
MX-25	5,380	5,530	6,300	6,510
MX-26	5,410	5,990	6,730	7,140
MX-27	5,330	5,730	6,310	6,680
MX-28	5,240	6,100	6,420	6,790
MX-37	4,160	4,320	5,160	6,110
MX-38	4,280	4,770	5,200	6,120
MX-39	4,260	4,780	5,380	6,160
MX-40	4,940	5,970	6,450	6,670

Table 4.6 summarizes the average compressive strength results of mixtures without any supplementary cementitious materials (No SCM). These mixtures exhibited a strength gain between 7 and 14 days, reaching values between 5,000 and 6,700 psi at 28 days. As the curing age extended to 56 days, the strength continued to increase, generally ranging from 6,000 to 7,100 psi. Mixtures with lower w/cm ratios, such as MX-3, MX-4, and MX-26, achieved the highest early-age and long-term strengths, indicating that reducing the w/cm ratio effectively enhanced hydration and matrix densification. Overall, the no-SCM mixtures exhibited a stable strength growth pattern, characterized by a gradual reduction in growth rate after 28 days.

Table 4.7 summarizes the average compressive strength results for concrete mixtures containing 25 percent fly ash. Compared to the cement-only group, the fly ash mixtures exhibited slightly lower early-age strengths at 7 and 14 days. At 28 days, most mixtures developed strengths ranging from 5,500 to 6,700 psi. However, significant late-age strength gains were observed, with several mixtures such as MX-5, MX-7, MX-31, and MX-32 exceeding 7,500 psi at 56 days, and the highest reaching 8,780 psi. This trend reflects the slower pozzolanic reactivity of fly ash at early ages but demonstrates its ability to enhance long-term strength and microstructural refinement through continued hydration.

Table 4.7: Average Compressive Strength of Mixtures Containing Fly Ash

Mix ID	Compressive Strength (psi)			
	7 Day	14 Day	28 Day	56 Day
MX-5	5,070	6,020	6,640	7,600
MX-6	4,630	5,070	5,600	7,130
MX-7	5,370	6,190	6,620	7,730
MX-8	5,330	5,600	6,540	6,930
MX-17	4,760	5,370	6,400	7,230
MX-18	4,120	4,820	5,820	6,160
MX-19	4,120	4,820	5,820	6,160
MX-20	4,880	5,830	6,440	7,490
MX-29	5,000	5,530	6,360	6,740
MX-30	5,160	5,860	6,870	7,450
MX-31	5,210	5,810	6,750	7,580
MX-32	5,240	6,040	7,010	8,780
MX-41	3,870	5,280	6,120	6,450
MX-42	4,150	4,810	6,610	6,490
MX-43	4,360	5,970	6,050	6,450
MX-44	5,150	5,560	6,270	6,980

Table 4.8 summarizes the average compressive strength results for concrete mixtures containing 25 percent GGBFS. The slag mixtures developed relatively lower early age strengths, with most values below 4,500 psi at 7 days. However, continuous strength growth was observed between 14 and 56 days. Several mixtures, including MX-10, MX-11, and MX-12, achieved strengths between 7,300 and 7,700 psi at 56 days, with an overall gain exceeding 2,000 psi after 28 days. These results indicate that GGBFS mixtures exhibit slower early hydration but substantial

long-term reactivity under extended curing, confirming their potential for improved durability and long-term performance.

Table 4.8: Average Compressive Strength of Mixtures Containing GGBFS

Mix IDs	Compressive Strength (psi)			
	7 Day	14 Day	28 Day	56 Day
MX-9	4,450	4,190	6,180	6,700
MX-10	4,730	5,490	6,610	7,670
MX-11	4,490	5,740	7,630	7,530
MX-12	4,690	5,850	6,600	7,340
MX-21	3,030	4,120	5,120	5,670
MX-22	3,580	4,920	5,730	6,240
MX-23	3,590	4,410	5,330	6,140
MX-24	3,300	4,410	5,340	5,730
MX-33	3,320	4,220	5,110	5,740
MX-34	3,830	4,710	5,270	6,110
MX-35	4,030	4,530	5,250	6,360
MX-36	4,020	5,010	5,600	6,910
MX-45	4,880	4,610	4,770	4,830
MX-46	4,940	4,450	4,830	5,420
MX-47	4,960	5,260	5,300	6,060
MX-48	4,570	4,600	5,040	5,720

4.5 Surface Resistivity Results

This section summarizes the results of surface resistivity testing conducted in accordance with KT-79, Surface Resistivity of Concrete Cylinders (KDOT, 2015). All specimens were prepared using the mixture proportions described in Chapter 3 and cured under standard conditions until the target testing age was reached. For each mixture, three cylindrical specimens with a diameter of 4 in. and a height of 8 in. were tested after curing for 7, 14, and 28 days. The measurements were performed using a Proceq Resipod four-probe resistivity meter with a probe spacing of 1.5 in. Before testing, each specimen surface was kept moist to ensure proper electrical contact. The reported surface resistivity meter (SRM) value, expressed in kilohms per centimeter (kΩ·cm), represents the average of four independent readings taken at four orientations on three samples.

Table 4.9: Average Surface Resistivity of Mixtures Without SCM.

Mix ID	Surface Resistivity (kΩ·cm)		
	7 Day	14 Day	28 Day
MX-1	9.3	9.9	10.6
MX-2	8.8	8.7	9.8
MX-3	7.2	8	8.2
MX-4	7.9	8.4	8.7
MX-13	6.8	7.2	8.1
MX-14	6.7	6.9	7.7
MX-15	6.3	7	8.8
MX-16	6.3	6.8	8.1
MX-25	7.4	8	9.7
MX-26	7.3	7.9	8.9
MX-27	7.2	8.2	9.2
MX-28	7.3	8	9.4
MX-37	6	6.6	7.2
MX-38	5.1	6.3	6.8
MX-39	5.4	5.7	6.4
MX-40	5.6	5.5	6.3

Table 4.9 summarizes the surface resistivity results of the mixtures without SCMs. These mixtures exhibited average resistivity values of 6-9 kΩ·cm at 7 days, with a consistent increase in resistivity as the mixture cured. By 28 days, most mixtures reached 8–10 kΩ·cm, and several low w/cm mixtures (0.38), such as MX-3, MX-4, and MX-26, exceeded 9.5 kΩ·cm. The overall trend indicates a gradual reduction in pore connectivity and ion transport pathways as hydration progressed.

Table 4.10 summarizes the surface resistivity results for mixtures containing 25 percent fly ash. The fly ash mixtures exhibited slightly lower early-age resistivity (approximately 5–7 kΩ·cm at 7 days) than the no-SCM mixtures, but showed a significant increase at later ages. At 14 days, most samples reached resistivities of 7–8 kΩ·cm, and by 28 days, the resistivity ranged from 9 to 12 kΩ·cm. Several mixtures, such as MX-5, MX-7, MX-31, and MX-32, exceeded 11 kΩ·cm at 28 days.

Table 4.10: Average Surface Resistivity of Mixtures Containing 25% Fly-Ash

Mix ID	Surface Resistivity (kΩ·cm)		
	7 Day	14 Day	28 Day
MX-5	6.5	7.7	11.6
MX-6	6	7.2	11.1
MX-7	6.1	7.8	12.1
MX-8	6.2	7.4	11
MX-17	6.1	7.1	10.5
MX-18	5.4	6.8	8.7
MX-19	5.5	6.2	8.4
MX-20	5.2	5.8	9.4
MX-29	6.4	7.6	11.4
MX-30	5.8	7.6	10.8
MX-31	6.3	7.2	11.2
MX-32	5.2	6.9	10.2
MX-41	4.8	6	9.4
MX-42	4.4	5.5	8.7
MX-43	4.3	5.4	8.3
MX-44	4.2	5.4	8.6

Table 4.11 summarizes the results for mixtures containing 25 percent GGBFS. The slag mixtures exhibited the highest growth rate among all binder systems, exhibiting average resistivity values of approximately 6 to 9 kΩ·cm at 7 days. By 14 days, most mixtures exceeded 12 kΩ·cm, and by 28 days, resistivity values ranged from 17 to 22 kΩ·cm. Some mixtures, such as MX-9, MX-10, MX-11, and MX-12, reached or exceeded 20 kΩ·cm at 28 days, indicating a higher resistance to ion migration in concrete with GGBFS.

Table 4.11: Average Surface Resistivity of Mixtures Containing 25% GGBFS

Mix ID	Surface Resistivity (kΩ·cm)		
	7 Day	14 Day	28 Day
MX-9	7.8	12.8	20.8
MX-10	8.5	11.8	20.1
MX-11	8.9	13.5	22
MX-12	7.2	12.9	22.9
MX-21	6.5	8.8	17.3
MX-22	6.7	11.2	17.1
MX-23	6.1	8.9	15.4
MX-24	5.9	9.6	16.3
MX-33	7.5	11.8	18.6
MX-34	7.5	12.4	21
MX-35	7.3	11.7	19.2
MX-36	6.7	11.3	19.2
MX-45	6.4	10.7	17
MX-46	6.3	10.4	16.7
MX-47	6	9.2	15.7
MX-48	6	9.6	16.9

Chapter 5: Model Validation

5.1 Overview

This chapter aims to validate the applicability of the dielectric constant–volumetric water content calibration models developed in Chapter 4, using TDR, for concrete mixtures in practice. To evaluate the accuracy and stability of the models across different material systems, two random trials were conducted at the KDOT Materials and Research Center, involving concrete mixing and testing. During each trial, measurements were taken simultaneously using the Phoenix System offered by Gilson, Inc. and the TDR measurement setup developed in this study. This allowed a direct comparison between the two methods in estimating the w/cm ratio and volumetric water content (θv) in fresh concrete. Two representative mixtures, designated as KDOT-1 and KDOT-2, were prepared based on KDOT's standard mixing practice. The primary control parameters included the w/cm ratio (0.40–0.44) and total cementitious material content. By comparing the Phoenix test results with the predicted values from the TDR-based calibration models, the reliability and error range of the four dielectric models developed in this study were evaluated. In addition, this chapter discusses the potential sources of error that may affect model prediction, including instrument noise, material heterogeneity, and environmental influences on dielectric measurements. The findings verify performance-based concrete quality control and support KDOT's efforts to implement TDR technology for field applications.

5.2 Experimental Setup in KDOT Laboratory

All experiments described in this section were conducted at the KDOT Laboratory in Topeka under controlled environmental conditions. Two representative mixtures, KDOT-1 and KDOT-2, were selected to evaluate the applicability of the TDR calibration models developed in this study and described in Chapter 4. Both mixtures were prepared and tested following the same procedures described in Chapter 3 to ensure experimental consistency.

Table 5.1 summarizes the mix KDOT-1, which was designed with a target water-to-cement ratio (w/cm) of 0.40. This blended system represents a potential pavement mixture with improved mechanical and long-term durability performance. The coarse aggregates consisted of Hamm

Eudora rocks, ½-inch Buildex, and 1/4-inch Buildex lightweight aggregates, and Hamm Silverlake sand was used as the fine aggregate. ADVA 140 was used as a water reducer, and DAIRAVAIR 1000 was added as an air-entraining admixture.

Table 5.1: Summary of KDOT-1 Mixture Design

Design Property			
Target w/cm			0.4
Design air content (%)			6
Design cement content (lb)			600
Cementitious Materials	Cement (%)		50
	Skyway slag (%)		46
	Skyway fly ash(%)		4
Aggregate	Coarse	Hamm Eudora (%)	25
		1/2" Buildex (%)	25
		¼" Buildex (%)	45
	Fine	Hamm Silverlake (%)	5
Admixtures	Water Reducer	ADVA 140 (oz/Cu.Yd.)	55
	Air Entrainment	DAIRAVAIR 1000 (oz/Cu.Yd)	3

Table 5.2 summarizes the KDOT-2 mix, which was designed as a fiber-reinforced concrete without supplementary cementitious materials. The target w/cm was 0.44, with a cement content of 600 lb/yd^3. The coarse aggregates consisted of Hayden and Trap Rock, and Hamm Silverlake sand was used as the fine aggregate. Additionally, 0.213 lb of Ace-60 acrylic microfiber was incorporated to enhance tensile strength and reduce cracking.

Table 5.2: Summary of KDOT-2 Mixture Design

Design Property			
Target w/cm			0.44
Design air content (%)			6
Design cement content (lb)			600
Aggregate	Coarse	Hayden (%)	30
		Trap Rock (%)	15
	Fine	Hamm Silverlake (%)	55
Additional	Ace-60 Acrylic Microfiber (lb)		0.213

Both mixtures were tested using the Phoenix System manufactured by Gilson, Inc. to obtain reference w/cm ratio level, and the TDR measurement system to determine dielectric constants for model comparison. Measurements were conducted within 10 minutes after mixing, and each batch was remixed before testing to ensure uniform water distribution.

5.3 Data Comparison

The measured Ka values from each mixture were converted into equivalent w/cm ratio for direct comparison between the TDR-based model predictions and the Phoenix results. The conversion process followed a sequential procedure. First, the measured Ka was standardized using the mean and standard deviation of each mixture group. The standardized Ka was then substituted into the calibration equations developed in Chapter 4 to obtain the predicted volumetric water content ($\text{logit}(\theta_v)$). The resulting logit (θ_v) values were transformed from logit space and converted into physical volumetric moisture content (θ_v).

To express this parameter in engineering terms, θ_v was multiplied by the specific weight of water (62.204 lb/ft^3) and the volume conversion factor (27 ft^3/yd^3) to obtain the total water content per cubic yard of concrete. Finally, this water content was divided by the cement content of the mixture (for example, 600 lb/yd^3) to calculate the equivalent w/cm ratio:

$$w/cm = \frac{\theta_v \times 62.204 \times 27}{c} \tag{5.1}$$

Where c is the cement content (lb/yd^3).

Table 5.3: Comparison of Results from TDR and Phoenix

Mix ID		KDOT-1	KDOT-2
Design w/cm		0.40	0.44
Measured Ka		19.978	20.01
Cement Content (lb/cy)		600	600
Calculated w/cm	Eq.4.3 All	0.4045	0.4049
	Eq.4.4 Cement Only	0.3975	0.3979
	Eq.4.5 Fly Ash	0.4021	0.4024
	Eq.4.6 GGBFS	0.4128	0.4131
Phoenix w/cm		0.40	0.43

Table 5.3 summarizes the comparison between the TDR-calculated w/cm ratio and the measured values obtained from the Phoenix System for mixtures KDOT-1 and KDOT-2. Both mixtures contained 600 lb/yd^3 of cement, with measured dielectric constants (Ka) of 19.978 and 20.01, respectively. These Ka values were substituted into the four calibration models developed in Chapter 4 (Eq. 4.3 to Eq. 4.6) to calculate the equivalent w/cm ratios.

For KDOT-1, the calculated w/cm values were 0.4045 (Eq. 4.3, All), 0.3975 (Eq. 4.4, Cement Only), 0.4021 (Eq. 4.5, Fly Ash), and 0.4128 (Eq. 4.6, GGBFS). Compared with the Phoenix reference value of 0.40, the fly ash model (Eq.4.5) provided the most accurate result, with an absolute error of +0.0021 (0.5% relative). The other models also performed well, with deviations within ±0.013, demonstrating consistent predictive performance.

For KDOT-2, the calculated results were 0.4049 (Eq. 4.3, ALL), 0.3979 (Eq. 4.4, Cement Only), 0.4024 (Eq. 4.5, Fly Ash), and 0.4131 (Eq. 4.6, GGBFS). Compared with the Phoenix value of 0.43, the GGBFS model (Eq.4.6) produced the closest prediction, with an absolute error of −0.0169 (3.9% relative). Although minor discrepancies exist among the four models, all predicted w/cm values remain within ±0.02 of the measured reference, confirming strong agreement.

5.4 Discussion of Model Reliability

In practical engineering applications, concrete mixtures often include multiple SCMs and admixtures, making it difficult for a single model to predict the dielectric behavior of all systems comprehensively. Each of the four calibration models developed in Chapter 4 (All, Cement Only, Fly Ash, and GGBF) demonstrated good fit for their respective material systems; however, when multiple SCMs or special additives are present, the accuracy of these models tends to decline.

For KDOT-2, the mixture contained not only conventional cementitious components but also Ace-60 acrylic microfibers. Compared with the Phoenix System measurements, the TDR-based models show slightly lower w/cm values. This difference could be due to the influence of fiber materials on dielectric behavior that was not included in the model framework. The introduction of fibers alters the microstructure and electric-field distribution of the cementitious matrix, thereby affecting the propagation velocity and reflection amplitude of the TDR signal.

Previous studies have shown that different types of fibers have opposite effects on the dielectric constant. Wang and Chung (1998) reported that carbon fibers significantly increase the overall dielectric constant of cementitious materials due to their electrical conductivity and strong interfacial polarization effect. In contrast, Chiarello and Zinno (2005) found that steel fibers tend to reduce the dielectric constant due to their metallic conductivity and localized shielding effect.

Therefore, when concrete contains materials not represented in the original model dataset, such as acrylic fibers, carbon fibers, or nano-reinforcing additives, the measured values may have systematic deviations from experimental measurements. In contrast, KDOT-1, which contained both GGBF and fly ash but no additional additives, showed excellent agreement between TDR predictions and Phoenix measurements. This agreement indicates that all four models can estimate w/cm with reasonable accuracy when the mixture composition falls within the calibrated system's range of validity.

Overall, the reliability of the TDR models depends on their applicability domain. Predictive uncertainty increases as material complexity exceeds the model's training boundaries. Future research should expand the experimental database to incorporate diverse admixtures and fiber-reinforced systems, thereby enhancing the model’s generalization capability and physical interpretability across different composite concrete mixtures.

Chapter 6 Conclusions and Recommendations

6.1 Conclusions

This study developed and validated a TDR-based method for estimating the w/cm ratio of fresh concrete. Laboratory testing and model calibration were conducted on 48 mixtures comprising different SCMs, varying cementitious materials, and varying air contents. The experimental results confirmed a consistent nonlinear relationship between the apparent dielectric constant and the volumetric water content, which formed the foundation for four calibrated models developed in this study: All-mix, Cement only, fly ash, and GGBFS.

The cement-only system achieved the highest coefficient of determination ($R^2 = 0.94$), while the fly ash and GGBFS models demonstrated acceptable reliability with R^2 values of 0.71 and 0.79, respectively. The All-mix model ($R^2 = 0.73$) effectively generalized the dielectric response across all mixture types. The SIMEX correction used in the R software environment successfully reduced measurement error bias and improved model stability, particularly in the high-moisture range.

Validation experiments conducted at the KDOT Materials Laboratory confirmed that the TDR-derived water-to-cement (w/cm) values closely matched those obtained from the Phoenix System, with deviations within ±0.02. This agreement demonstrates that TDR can serve as a rapid, non-destructive, and reliable technique for estimating the effective water content in fresh concrete. Moreover, the results indicated that TDR measurements are sensitive to mixture composition, especially when multiple SCMs or fibers are present, which may cause systematic deviations if not accounted for in the calibration.

6.2 Recommendations

Based on the findings of this study, several recommendations are proposed to improve further the accuracy, applicability, and engineering performance of the TDR-based calibrated models. Future research should expand the dataset to include a broader range of concrete mixtures containing multiple SCMs and chemical admixtures, thereby enhancing the model's generalization capability. In addition, the dielectric behavior of fiber-reinforced concrete should be systematically

investigated, as the current model does not account for the polarization effects introduced by materials such as acrylic, carbon, or steel fibers. Moreover, since this study utilized a fixed-frequency TDR instrument, future work should also examine the frequency-dependent dielectric responses of cementitious materials to better capture the dynamic signal behavior. Integrating the empirical regression models with physics-based dielectric models could further strengthen the theoretical foundation of the method. The long-term stability, durability, and environmental sensitivity of TDR sensors under construction conditions—such as temperature, humidity, and electrical conductivity—should also be evaluated, and field-deployable TDR systems should be developed for practical use. In summary, future research should advance along three main directions: model expansion, investigation of physical mechanisms, and engineering validation, to achieve standardization and practical implementation of TDR technology in concrete quality monitoring and performance evaluation.

References

AASHTO. (2019). Standard Method of Test for Surface Resistivity Indication of Concrete's Ability to Resist Chloride Ion Penetration (T 358). American Association of State Highway and Transportation Officials.

Acclima. (2017). Acclima TDR-315 Sensor User Manual. Acclima Inc.

ACI Committee 211. (2002). Standard Practice for Selecting Proportions for Normal, Heavyweight, and Mass Concrete (ACI 211.1). American Concrete Institute.

ACI Committee 212. (2010). Report on Chemical Admixtures for Concrete (ACI 212.3R). American Concrete Institute.

ACI Committee 225. (2019). Guide to the Selection and Use of Hydraulic Cements (ACI 225R-19). American Concrete Institute.

ASTM. (2018). ASTM C33: Standard Specification for Concrete Aggregates. ASTM International.

ASTM. (2023). ASTM C231: Standard Test Method for Air Content of Freshly Mixed Concrete by the Pressure Method. ASTM International.

ASTM. (2024a). ASTM C127: Standard Test Method for Density, Relative Density (Specific Gravity), and Absorption of Coarse Aggregate. ASTM International.

ASTM. (2024b). ASTM C128: Standard Test Method for Density, Relative Density (Specific Gravity), and Absorption of Fine Aggregate. ASTM International.

Berini, C. M., Janoo, V. C., & Korhonen, C. J. (1997). Time-domain reflectometry of water content in Portland cement concrete (CRREL Special Report 97-27). U.S. Army Cold Regions Research and Engineering Laboratory, Hanover, NH.

Breusch, T. S., & Pagan, A. R. (1979). A Simple Test for Heteroscedasticity and Random Coefficient Variation. *Econometrica, 47*(5), 1287–1294. https://doi.org/10.2307/1911963

Carroll, R. J., Ruppert, D., Stefanski, L. A., & Crainiceanu, C. M. (2006). Measurement Error in Nonlinear Models: A Modern Perspective (2nd ed.). Chapman and Hall/CRC.

Cataldo, A., De Benedetto, E., Cannazza, G., Piuzzi, E., & Pittella, E. (2018). TDR-based measurements of water content in construction materials for in-the-field use and calibration.

IEEE Transactions on Instrumentation and Measurement, 67(5), 1230–1237. https://doi.org/10.1109/TIM.2017.2770778

Cook, J. R., & Stefanski, L. A. (1994). Simulation-extrapolation estimation in parametric measurement error models. *Journal of the American Statistical Association*, 89(428), 1314–1328.

FHWA. (2016). Supplementary cementitious materials (Tech Brief HIF-16-001). Federal Highway Administration

Gilson Co. (n.d.). Concrete Phoenix Furnace System and App. Retrieved [2025], from Gilson Company, Inc.

Gilson Co. (n.d.). Concrete Slump Test—A Guide to the Test Procedure. Retrieved [2025], from Gilson Company, Inc.

Greene, W. H. (2018). *Econometric Analysis* (8th ed.). Pearson Education.

Haddad, A. S., & Chung, D. D. L. (2017). Decreasing the electric permittivity of cement by graphite particle incorporation. Carbon, 122, 702–709. https://doi.org/10.1016/j.carbon.2017.06.088

Issa, I. M., Zollinger, D. G., Onifade, I., & Lytton, R. L. (2022). Laboratory approach to determine roller compacted concrete mixture electrical characteristics using a new time-domain reflectometry interpretation method. Transportation Research Record, 2676(1), 376–387. https://doi.org/10.1177/03611981211036370.

KDOT. (2015a). Standard Specifications for State Road and Bridge Construction. Kansas Department of Transportation.

KDOT. (2015b). Standard Specifications for State Road and Bridge Construction. Kansas Department of Transportation. Section 1116, Aggregates for On-Grade Concrete, Kansas Department of Transportation.

KDOT. (2020). KT-18: Slump of Hydraulic Cement Concrete. Kansas Department of Transportation.

KDOT. (2015c). KT-19: Air Content of Freshly Mixed Concrete by the Pressure Method. Kansas Department of Transportation.

KDOT. (2018). KT-76: Compressive Strength of Cylindrical Concrete Specimens. Kansas Department of Transportation.

KDOT. (2015d). KT-79: Surface Resistivity of Hardened Concrete Cylinders. Kansas Department of Transportation.

Krishnamoorthy, A., Nomura, K.-i., Baradwaj, N., Shimamura, K., Rajak, P., Mishra, A., Fukushima, S., Shimojo, F., Kalia, R., Nakano, A., & Vashishta, P. (2021). Dielectric constant of liquid water determined with neural network quantum molecular dynamics. Physical Review Letters, 126, 216403. https://doi.org/10.1103/PhysRevLett.126.216403

Kosmatka, S. H., Kerkhoff, B., & Panarese, W. C. (2011). Design and Control of Concrete Mixtures (15th ed.). Portland Cement Association.

Ley, T., & Masten, J. (2023). Testing the w/cm of fresh concrete with the Phoenix [Slides]. Institute for Transportation, Iowa State University.

Mardmomen, S., Chen, H.-L., & Leon, G. (2019). Revised method for rapid determination of on-site water–cement ratio using microwave oven. Transportation Research Record, 2673(8), 1–10. doi:10.1177/0361198119849408

Mehta, P. K., & Monteiro, P. J. M. (2014). Concrete: Microstructure, Properties, and Materials (4th ed.). McGraw-Hill Education.

Mindess, S., Young, J. F., & Darwin, D. (2003). Concrete (2nd ed.). Prentice Hall.

Montgomery, D. C., Peck, E. A., & Vining, G. G. (2021). *Introduction to Linear Regression Analysis* (6th ed.). Wiley.

Neville, A. M. (2011). Properties of Concrete (5th ed.). Pearson Education Limited.

Ojala, T., & Punkki, J. (2024). Automatic Measurement Techniques for Compositional Properties of Fresh Concrete: Focus on Water/Cement Ratio and Air Content. Nordic Concrete Research, 71(2), 91–110. https://doi.org/10.2478/ncr-2024-0015

R Core Team. (2024). R: A Language and Environment for Statistical Computing. R Foundation for Statistical Computing.

Robinson, D. A., Jones, S. B., Wraith, J. M., Or, D., & Friedman, S. P. (2003). A review of advances in dielectric and electrical conductivity measurement in soils using time domain reflectometry. *Vadose Zone Journal*, 2(4), 444–475. https://doi.org/10.2136/vzj2003.4440

Saha, O., Boulfiza, M., & Wegner, L. D. (2020). Tracking the hydration of antifreeze-treated cement paste at subfreezing temperatures using the TDR technique. Construction and Building Materials, 262, 119915. https://doi.org/10.1016/j.conbuildmat.2020.119915

Topp, G. C., Davis, J. L., & Annan, A. P. (1980). Electromagnetic determination of soil water content: Measurements in coaxial transmission lines. *Water Resources Research*, 16(3), 574–582. https://doi.org/10.1029/WR016i003p00574

Bechtel, A. J., & Al-Omaishi, N. (2016). Determination of water–cement ratio of fresh concrete using water content found through microwave oven method. Paper presented at the Transportation Research Board 95th Annual Meeting. Retrieved from https://trid.trb.org/View/1392402

Williams, E. J. (1959). *Regression Analysis*. John Wiley & Sons.

Wooldridge, J. M. (2019). *Introductory Econometrics: A Modern Approach* (7th ed.). Cengage Learning.

Yu, X. (B.), & Liu, Y. (2010). Development of time domain reflectometry instrument for QA/QC of fresh and early-stage concrete (Highway IDEA Project 126, Final Report). Transportation Research Board of the National Academies.

Zheng, Y., Su, Z., Fu, H., Zhang, Q., & Li, J. (2024). Thermal behaviors of cement and mortar under microwave treatment and the influencing factors: An experimental study. Construction and Building Materials, 411, 134191. https://doi.org/10.1016/j.conbuildmat.2023.134191

Appendix A: Complete Mixing Matrix

Table A.1: Mixing Matrix for 48 Mixtures

Mix ID	Target w/cm	Design Cement Content (lb/cy)	Cement (%)	SCM (%)	Design Air Content (%)
MX-1	0.38	500	100% BUZZ IL	None	5.00%
MX-2	0.38	530	100% BUZZ IL	None	5.00%
MX-3	0.38	560	100% BUZZ IL	None	5.00%
MX-4	0.38	590	100% BUZZ IL	None	5.00%
MX-5	0.38	500	75% BUZZ IL	25% C Jeff Fly-Ash	5.00%
MX-6	0.38	530	75% BUZZ IL	25% C Jeff Fly-Ash	5.00%
MX-7	0.38	560	75% BUZZ IL	25% C Jeff Fly-Ash	5.00%
MX-8	0.38	590	75% BUZZ IL	25% C Jeff Fly-Ash	5.00%
MX-9	0.38	500	75% BUZZ IL	25% Skyway Slag	5.00%
MX-10	0.38	530	75% BUZZ IL	25% Skyway Slag	5.00%
MX-11	0.38	560	75% BUZZ IL	25% Skyway Slag	5.00%
MX-12	0.38	590	75% BUZZ 1L	25% Skyway Slag	5.00%
MX-13	0.44	500	100% BUZZ IL	None	5.00%
MX-14	0.44	530	100% BUZZ IL	None	5.00%
MX-15	0.44	560	100% BUZZ IL	None	5.00%
MX-16	0.44	590	100% BUZZ IL	None	5.00%
MX-17	0.44	500	75% BUZZ IL	25% C Jeff Fly-Ash	5.00%
MX-18	0.44	530	75% BUZZ IL	25% C Jeff Fly-Ash	5.00%

Table A.1: Mixing Matrix for 48 Mixtures Continue

MX-19	0.44	560	75% BUZZ IL	25% C Jeff Fly-Ash	5.00%
MX-20	0.44	590	75% BUZZ IL	25% C Jeff Fly-Ash	5.00%
MX-21	0.44	500	75% BUZZ IL	25% Skyway Slag	5.00%
MX-22	0.44	530	75% BUZZ IL	25% Skyway Slag	5.00%
MX-23	0.44	560	75% BUZZ IL	25% Skyway Slag	5.00%
MX-24	0.44	590	75% BUZZ 1L	25% Skyway Slag	5.00%
MX-25	0.38	500	100% BUZZ IL	None	10.00%
MX-26	0.38	530	100% BUZZ IL	None	10.00%
MX-27	0.38	560	100% BUZZ IL	None	10.00%
MX-28	0.38	590	100% BUZZ IL	None	10.00%
MX-29	0.38	500	75% BUZZ IL	25% C Jeff Fly-Ash	10.00%
MX-30	0.38	530	75% BUZZ IL	25% C Jeff Fly-Ash	10.00%
MX-31	0.38	560	75% BUZZ IL	25% C Jeff Fly-Ash	10.00%
MX-32	0.38	590	75% BUZZ IL	25% C Jeff Fly-Ash	10.00%
MX-33	0.38	500	75% BUZZ IL	25% Skyway Slag	10.00%
MX-34	0.38	530	75% BUZZ IL	25% Skyway Slag	10.00%
MX-35	0.38	560	75% BUZZ IL	25% Skyway Slag	10.00%
MX-36	0.38	590	75% BUZZ 1L	25% Skyway Slag	10.00%
MX-37	0.44	500	100% BUZZ IL	None	10.00%
MX-38	0.44	530	100% BUZZ IL	None	10.00%
MX-39	0.44	560	100% BUZZ IL	None	10.00%

Table A.1: Mixing Matrix for 48 Mixtures Continue

MX-40	0.44	590	100% BUZZ IL	None	10.00%
MX-41	0.44	500	75% BUZZ IL	25% C Jeff Fly-Ash	10.00%
MX-42	0.44	530	75% BUZZ IL	25% C Jeff Fly-Ash	10.00%
MX-43	0.44	560	75% BUZZ IL	25% C Jeff Fly-Ash	10.00%
MX-44	0.44	590	75% BUZZ IL	25% C Jeff Fly-Ash	10.00%
MX-45	0.44	500	75% BUZZ IL	25% Skyway Slag	10.00%
MX-46	0.44	530	75% BUZZ IL	25% Skyway Slag	10.00%
MX-47	0.44	560	75% BUZZ IL	25% Skyway Slag	10.00%
MX-48	0.44	590	75% BUZZ 1L	25% Skyway Slag	10.00%

Appendix B: Model Diagnostics Plots

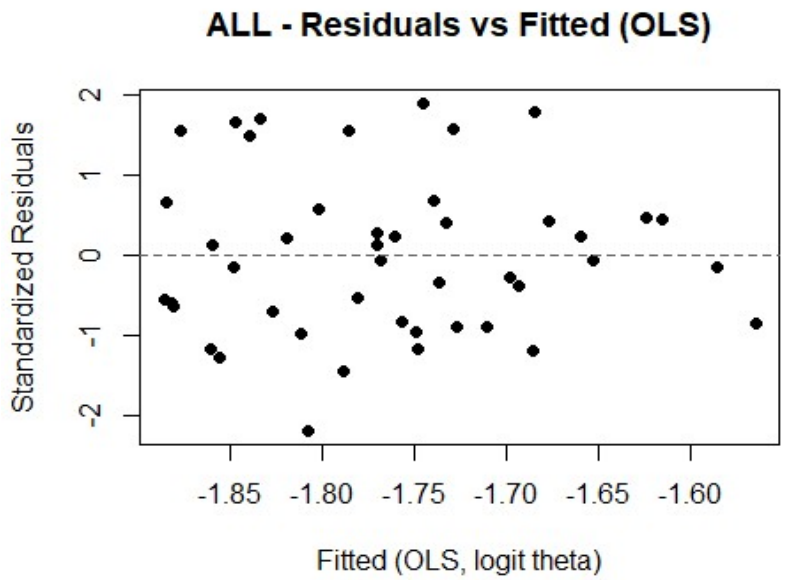

Figure B.1: Residuals versus fitted values plot for all mixtures

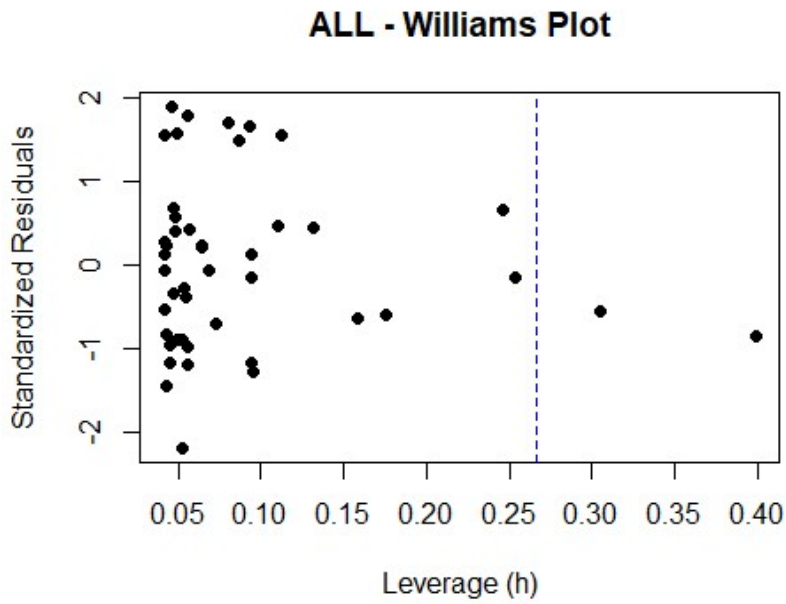

Figure B.2: Williams plot for all mixtures

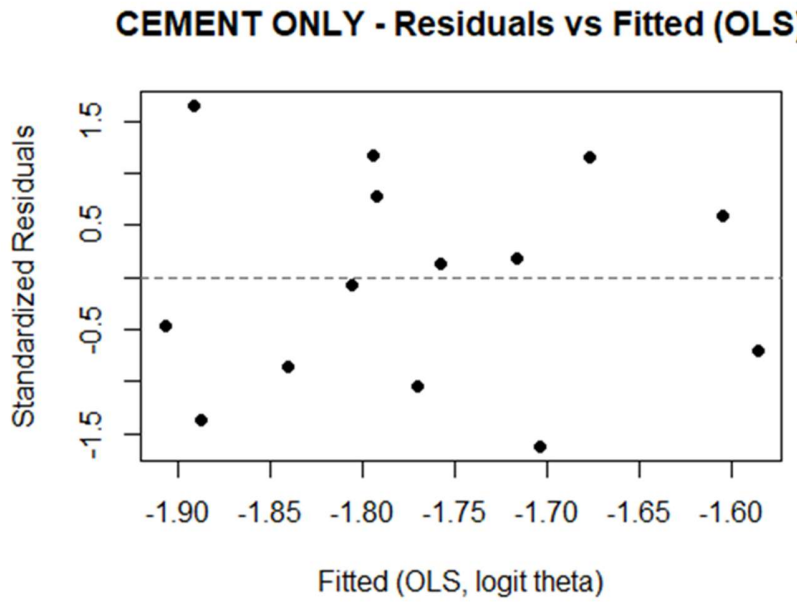

Figure B.3: Residuals versus fitted values plot for cement-only mixtures

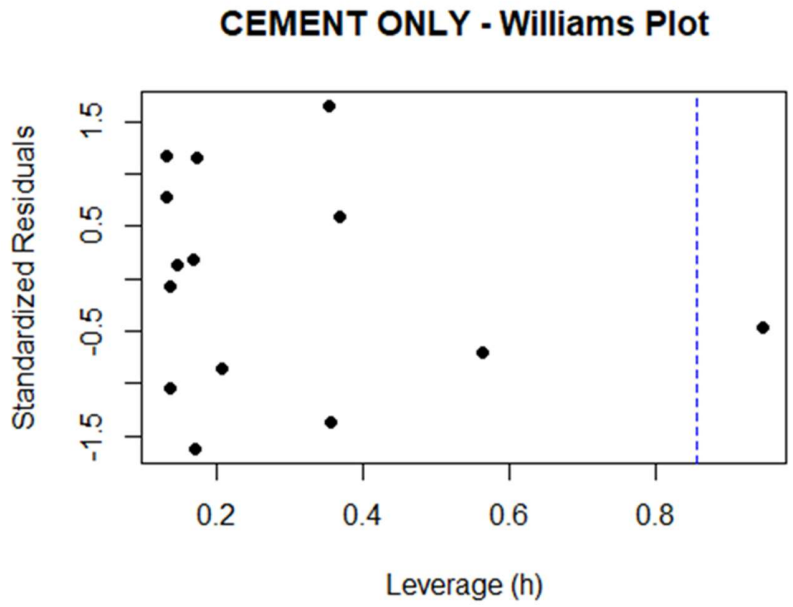

Figure B.4: Williams plot for cement-only mixtures

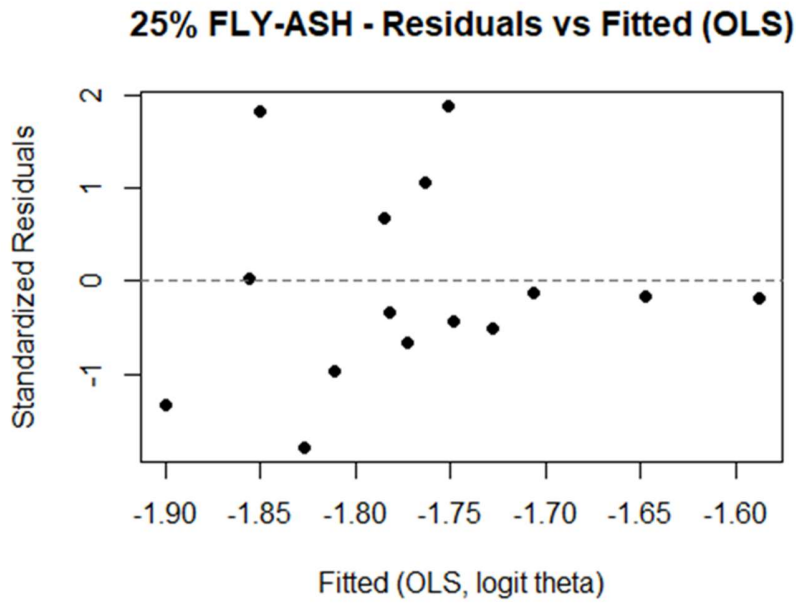

Figure B.5: Residuals versus fitted values plot for 25% fly ash replacement mixtures

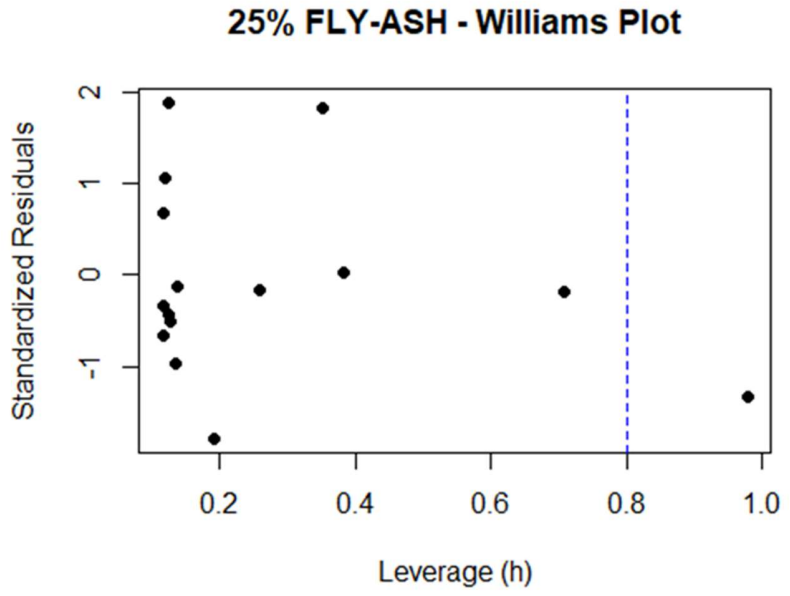

Figure B.6: Williams plot for 25% fly ash replacement mixtures

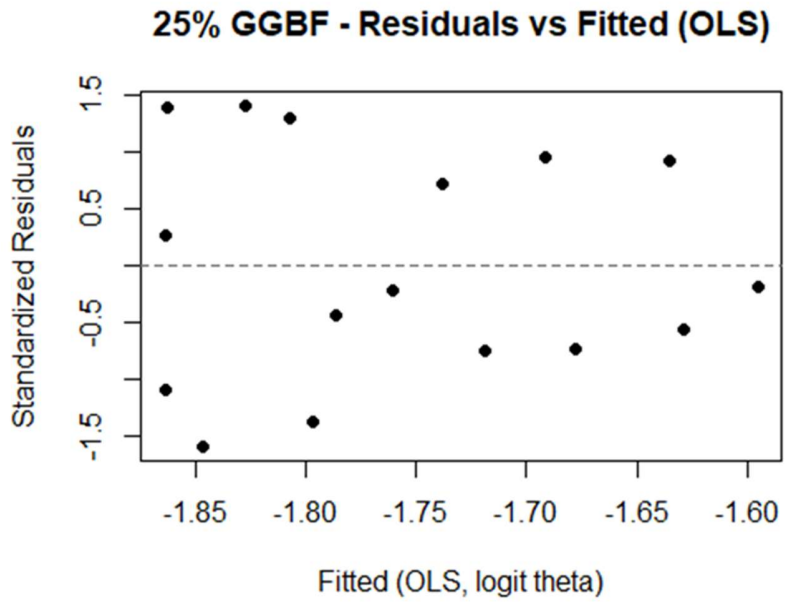

Figure B.7: Residuals versus fitted values plot for 25% GGBF replacement mixtures

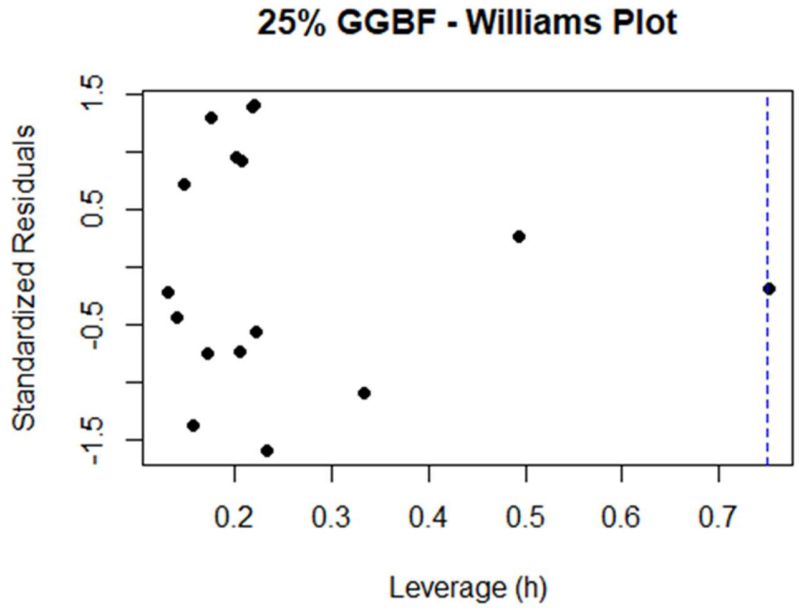

Figure B.8: Williams plot for 25% GGBF replacement mixtures